ORIGINAL PAPER

CrossMark

Optimization of salt concentration and explanation of two peak percolation in blend solid polymer nanocomposite films

Anil Arya[1] · A. L. Sharma[1]

Abstract

The present paper is focused toward the preparation of the flexible and free-standing blend solid polymer electrolyte films based on PEO-PVP complexed with $NaPF_6$ by the solution cast technique. The structural/morphological features of the synthesized polymer nanocomposite films have been investigated in detail using X-ray diffraction, Fourier transform infra-red spectroscopy, Field emission scanning electron microscope, and Atomic force microscopy techniques. The film PEO-PVP + $NaPF_6$ ($\ddot{O}/Na^+ = 8$) exhibits highest ionic conductivity $\sim 5.92 \times 10^{-6}$ S cm^{-1} at 40 °C and $\sim 2.46 \times 10^{-4}$ S cm^{-1} at 100 °C. The temperature-dependent conductivity shows an Arrhenius type behavior and activation energy decreases with the addition of salt. The high temperature (100 °C) conductivity monitoring is done for the optimized PEO-PVP + $NaPF_6$ ($\ddot{O}/Na^+ = 8$) highly conductive system and the conductivity is still maintained stable up to 160 h (approx. 7 days). The thermal transitions parameters were measured by the differential scanning calorimetry (DSC) measurements. The prepared polymer electrolyte film displays the smoother surface on addition of salt and a thermal stability up to 300 °C. The ion transference number (t_{ion}) for the highest conducting sample is found to be 0.997 and evidence that the present system is ion dominating with negligible electron contribution. Both linear sweep voltammetry and cyclic voltammetry supports the use of prepared polymer electrolyte with long-term cycle stability and thermal stability for the solid-state sodium ion batteries. Finally, a two peak percolation mechanism has been proposed on the basis of experimental findings.

Keywords Blend polymer electrolyte · Electrical conductivity · Activation energy · Two peak percolation mechanism · Transport parameters

Introduction

The most challenging and discussible issue is the search of the sustainable and appropriate source of energy that can fulfill the

Highlights
• Solid polymer electrolytes based on PEO-PVP complexed with $NaPF_6$ are prepared.
• XRD, AFM, FESEM, and FTIR techniques have been performed.
• The prepared system reveals superior ionic conductivity and long-term stability.
• Temperature-dependent conductivity shows an Arrhenius nature.
• Correlation between the T_g, T_m, transport parameters and ionic conductivity is presented.
• A two peak percolation mechanism has been proposed.

✉ A. L. Sharma
  alsharma@cup.edu.in

[1] Centre for Physical Sciences, Central University of Punjab, Punjab, Bathinda 151001, India

increasing global demand. The use of renewable and cleaner energy sources, such as solar radiation, wind, and waves, is flattering as a key source of energy which can amend the dependency on the non-renewable sources of energy (fossil fuels) and will lower the global temperature by 2 °C. The most attractive and suitable candidate for the clean and efficient energy source is secondary batteries such as a lithium-ion battery (LIB) and sodium ion battery (SIB). The former one is the main thrust area of research and mostly used in the cellular phone, personal computers, electric vehicles, hybrid electric vehicle, and other digital portable products due to high specific energy and power. LIB has associated issues such as safety, lack of abundance, and high cost. So, to develop an alternative abundant, cheap, stable, and non-toxic energy storage system has pushed forward R&D on SIB and demonstrating itself as a potentially more convenient alternative to existing LIB [1–3]. Due to the increasing global demand for energy, SIB research boosted itself due to the abundance (sixth most abundant element in earth crust, 2.64%), readily accessible in both earth-

crust/ocean, high reduction potential (− 2.7 V), low toxicity, low cost (seven times lower than lithium), softness, and atomic mass. To meet the global demand for energy, now research is focused on the development of sodium ion-based devices due to the uniform geographical distribution of sodium [4–12].

A conventional battery is comprised of a cathode, anode, separator, and electrolyte. Both cathode and anode are the accommodating sites for the ions. The separator role is to physically separate the electrodes while the electrolyte provides the medium to the ions shuttling between electrodes. At present, the liquid electrolyte is used in commercial systems and that limits its geometry and application range due to an associated drawback such as leakage of organic solvents, flammability, short-circuit issue, poor mechanical properties, and incompatibility with high-energy batteries. So, there is need of suitable electrolyte cum separator with desirable ionic conductivity and the long cycle stability enabling better performance. The polymer electrolytes are alternate to the liquid electrolyte and are attempted since the first report by Fenton et al., [13] in 1973. Then, in 1978, polymer electrolytes were proposed first time for application in batteries due to the advantage of both solid-state electrochemistry and easy preparation [14]. Then, gel polymer electrolyte (GPE) prepared by incorporation of the plasticizer emerged as an attractive candidate due to good compatibility with liquid electrolyte but poor mechanical property, interfacial properties, and deficiency of shutdown behavior was a bigger constraint for commercial applications [15]. Solid polymer electrolytes (SPEs) are the potential candidate to overcome the above-said drawback associated with the traditional liquid and gel polymer electrolyte. So, in order for the replacement of liquid and gel polymer electrolyte completely, SPE must possess desirable ionic conductivity, enhanced thermal, electrochemical and mechanical stability. One major advantage with the SPE is the simple & low-cost design strategy, flexibility, and miniaturization of devices that automatically lowers both cost and weight. As no liquid part is used, so all solid-state battery guarantees great safety than the existing one [16, 17]. SPE also plays a dual role in energy storage/conversion devices. It permits the transportation of ionic charge carriers as well as prevents electrical short circuits between the electrodes. So, various polymer materials have been studied and developed as SPE matrix [18–23].

Poly(ethylene oxide) is one of the most auspicious candidates since the last three decades due to its low glass transition temperature, the good capability to dissolve salts, high ionic conductivity, and high degradation temperature. The presence of the electron donor ether group ($CH_2-\ddot{O}-CH_2$) in polymer backbone ($-CH_2-CH_2-\ddot{O}-$) makes it fascinating for coordination with the available cations and favor enhanced polymer segmental motion. However, the semi-crystalline nature of PEO is responsible for low ionic conductivity, and poor mechanical strength hinders its usage in SPEs. Various strategies have been adopted to improve the inclusive performance of PEO-based electrolytes by modifying the structure of the PEO. Since it is well proven that enormous amorphous phase favors easier and smoother cation migration in such ion conducting system [24–27]. Therefore, the polymer blending approach is tried to make such system more amorphous and appears appropriate in improving the compromised parameters during use of a semi-crystalline polymer as host materials. Polymer blends are obtained by physical mixing of two or more polymers without any chemical reaction among them. One sole advantage of the blending approach is appropriateness to control over the properties by varying the material composition and easiest means of preparation. Recently, many efforts have been devoted in enhancing the electrochemical and mechanical properties in blend solid polymers electrolytes (BSPE) membranes such as PEO-PAN, PVdF-PEO, PEO-PVdF, PVA-PEO, PEO-PEG, PVA-PVP, PVC-PEMA, PVC-PVdF, PEO-PVP, PEO-P(VdF-HFP), and PVC-PEO [28–42].

Poly(vinyl pyrrolidone) (PVP) has some remarkable properties that motivated us for its selection as the partner with PEO (semi-crystalline polymer) in the preparation of blend polymer electrolyte (BPE). It possesses moderate electrical conductivity, good environmental stability, rich physics in charge transport mechanism, and easiest way of preparation. Also, the high amorphous content associated with it validates its candidature. The presence of the rigid pyrrolidone group in amorphous PVP helps to provide better ionic mobility in these systems and carbonyl group (C=O) attached to the side chains of PVP helps in the formation of a number of complexes with different inorganic salts [43–46].

Doping of sodium salt in existing technology (lithium based electrolyte) overcomes the other issues like smaller cations such as lithium capturing probability by the polymer network are more and that lowers the ion mobility [47]. Another advantage of the sodium is that its softness nature makes the smooth and proper contact with the electrochemical devices. The ionic conducting properties of PEO, doped with different sodium salts like sodium perchlorate ($NaClO_4$), sodium fluoride (NaF), sodium iodide (NaI), sodium bromide (NaBr), sodium hexafluoro phosphate ($NaPF_6$), sodium periodate ($NaIO_4$), and sodium tetrafluoroborate ($NaBF_4$) have already been reported in literature [10, 46, 48–55]. So, after reviewing the various sodium-based solid polymer electrolyte systems, sodium hexafluoro phosphate ($NaPF_6$) is selected as the cation (Na^+) source for doping PEO/PVP-based blend solid polymer electrolyte. The current report is focused toward the search of suitable SPE by the complexation of $NaPF_6$ with blend PEO-PVP. So, here, the advantage of flexible high solvation matrix of PEO and amorphous content of PVP for sodium ions are utilized for developing the blend solid polymer electrolyte [56–59] system.

As per author finding, there are not any studies based on $NaPF_6$ incorporated PEO/PVP-based blend polymer electrolyte for the development of flexible and freestanding SPE films. So,

in the present investigation, the optimum concentration of $NaPF_6$ in PEO/PVP blend polymer is obtained to develop good quality free standing SPE films. First, the structural, surface, and microstructural investigations are established by X-ray diffraction (XRD), field emission scanning electron microscopy (FE-SEM), atomic force microscopy (AFM), and Fourier transformation infra-red spectroscopy (FTIR). Thermo-gravimetric analysis (TGA) is used to find the thermal stability of the synthesized film sample and differential scanning calorimetry (DSC) to find the glass transition temperature and crystallinity of all SPEs. The ionic conductivity of the prepared solid polymer electrolyte samples at different temperatures is measured using an electrochemical analyzer set up. The ion transference number of the electrolyte film is estimated using the dc polarization method. The linear sweep voltammetry (LSV) and cyclic voltammetry (CV) were characterized for obtaining the voltage window of the electrolyte and also the temperature dependency of the voltage window was observed.

To get a better insight on the cation transport within the electrolytes, the correlation between the estimated transport parameters with electrical parameters has also been analyzed. Finally, a mechanism is proposed that supports the experimental findings.

Experimental

Materials

PEO (M_w = 200,000), PVP (M_w = 40,000), and $NaPF_6$ (M_w = 167.95 g/mol) were purchased from Sigma-Aldrich, India, and used as received. The chemical structure of all material is displayed in Fig. 1. The solvent methanol was purchased from Lobha Chemicals, India. The standard solution cast technique was used for the preparation of the PEO-PVP + $NaPF_6$ complex with methanol as common solvent.

Preparation of PEO-PVP + $NaPF_6$-based solid polymer electrolyte

The concentration of PEO and PVP were kept constant 80:20 for all solid polymer electrolytes. The addition of an appropriate amount of salt ($NaPF_6$) stoichiometric ratio has been calculated considering oxygen of PEO. The formula for this calculation is shown below.

For PEO:

$$\frac{\ddot{O}}{Na^+} = \frac{No.\ of\ monomer\ unit\ in\ 0.4\ gram\ of\ PEO}{No.\ of\ NaPF_6\ molecule\ in\ half\ gram\ of\ salt}$$

$$\times \frac{wt.of\ PEO\ took}{wt.of\ salt\ is\ taken}$$

The salt concentration ($\ddot{O}/Na^+$) was varied as $\ddot{O}/Na^+$ = 2, 4, 6, 8, 10.

First of all, PEO and PVP were added in methanol (20 ml) and kept for 10 min for swelling of polymer chains. Then, stirring was done for 4 h at room temperature, until a completely transparent and homogeneous solution was obtained. Then, the appropriate stoichiometric ratio of salt ($\ddot{O}/Na^+$ = 2, 4, 6, 8, 10) was added and stirring was done again for 12 h at room temperature. The final homogenous solution obtained was cast in the petri dishes and kept at room temperature in a desiccator (silica gel inside) to avoid forming any moisture content. Then, after evaporation of the solvent, for complete removal of solvent, petri dishes were kept in a vacuum oven at 60 °C for 24 h. Finally, the free-standing solid polymer electrolyte films were obtained after peeling off from the petri dish. The prepared film was stored in a desiccator to avoid contamination and for further relevant characterizations. The blend formation interaction mechanism (Fig. 2a) along with a snapshot of solution cast technique is depicted in Fig. 2b.

Characterization

X-ray diffraction (XRD) (Bruker D8 Advance) was performed for the determination of crystallinity and recorded with Cu-K_α radiation (λ = 1.54 Å) in the Braggs angle range (2θ) from 10 to 60°. Field emission scanning electron microscopy (FESEM) was used to study the surface morphology (FESEM: Carl Zeiss product) and taken in a high vacuum after sputtering the samples with gold in order to prepare conductive surfaces. The Fourier transform infrared (FTIR) spectra (Bruker Tensor 27, Model: NEXUS–870) were recorded in absorbance mode over the wave number region from 600 to 3500 cm^{-1} (resolution of 4 cm^{-1}) to probe the presence of various microscopic interactions such as polymer-ion, ion-ion interaction, and complex formation. The ionic conductivity was measured by impedance spectroscopy (IS) in the frequency range of 1 Hz to 1 MHz using the CHI 760 electrochemical analyzer. An AC sinusoidal signal of 10 mV was applied to the cell configuration SS|SPE|SS where solid polymer electrolyte films were sandwiched between two stainless steel (SS) electrodes. The intercept between the semi-circle at high frequency and tilted spike at low frequency were taken as the bulk resistance (R_b). The electrical conductivity (σ) value was obtained using Eq. 1:

$$\sigma_{dc} = \frac{1}{R_b}\frac{t}{A} \qquad (1)$$

where "t" is thickness (cm) of the polymer film (100–125 μm), R_b is bulk resistance (Ω), and A is area (cm^2) of the working electrode (1.43 cm^2). The variation of ionic conductivity of the electrolyte film with temperature was studied in the temperature range from 40 to 100 °C with a temperature difference of 10 °C (Temperature Controller; Marine India). The thermal activation energy for ionic transport was

Fig. 1 Structure unit of PEO, PVP, and salt NaPF$_6$
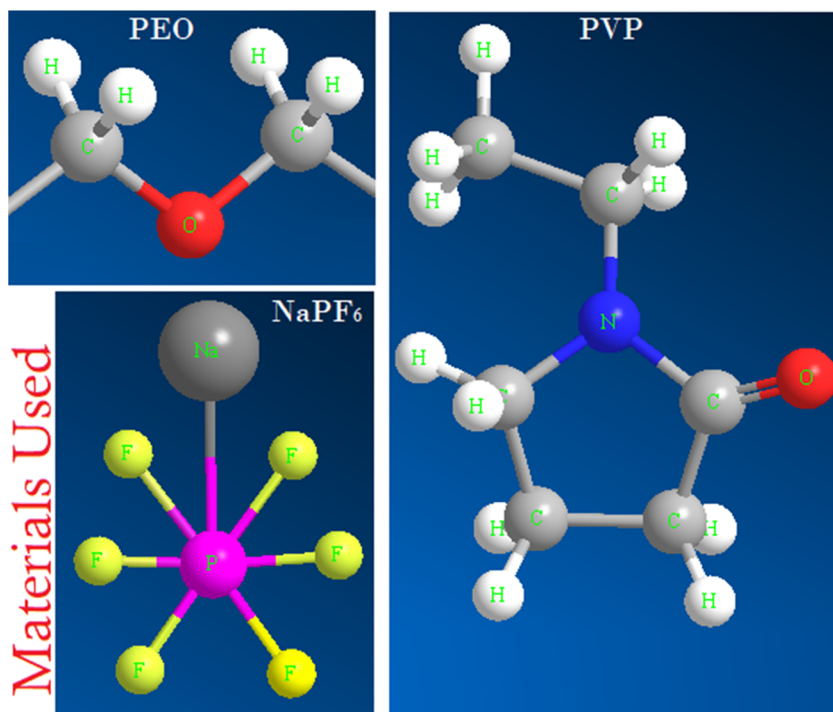
estimated from the slope of the linear fit of the Arrhenius plot. The linear variation in log ($\sigma/S\ cm^{-1}$) vs. 1000/T plot suggests a thermally activated process represented by $\sigma = \sigma_o\ exp\ (-E_a/kT)$, where σ_o is the constant pre-exponential factor and E_a is the activation energy. The parameter T stands for the absolute temperature and k for the Boltzmann constant.

Differential scanning calorimetry (DSC) measurements were performed to find the glass transition temperature, melting temperature, and crystallinity of all SPEs with a heating rate of 10 °C min^{-1} from − 100 to 100 °C under an N$_2$/Ar atmosphere (DSC-Sirius 3500). SPEs films with the weight of 8–10 mg were sealed in aluminum pans, and an empty
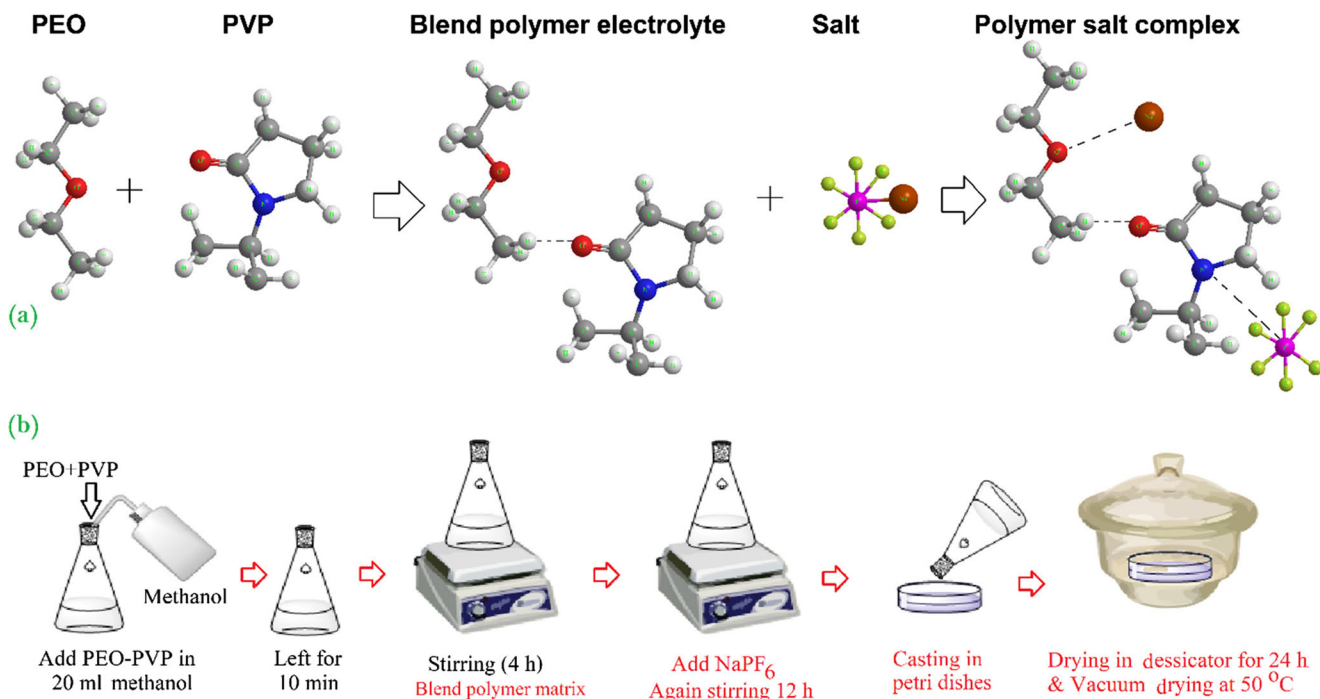

Fig. 2 **a** Representation of blend formation and cation coordination. **b** Flow chart of solution cast technique

sealed aluminum pan was used as a reference. The total ionic transference number (t_{ion}) was obtained by placing polymer electrolyte film between stainless steel (SS) blocking electrodes and a fixed dc voltage of 10 mV was applied across the $SS|SPE|SS$ cell. Ion transference numbers of the solid polymer electrolytes was evaluated using Eq. 2 on $SS|SPE|SS$ cell:

$$t_{ion} = \left(\frac{I_t - I_e}{I_t}\right) \times 100 \qquad (2)$$

The prepared polymer electrolytes have also been subjected to atomic force microscopy (AFM, Veeco CP-II) surface image studies. Thermal stability of the synthesized SPE films was investigated using thermo-gravimetric analysis (TGA–SHIMADZU–DTG-60H) under dynamic temperature conditions from 30 to 600 °C, in a controlled nitrogen atmosphere at a constant heating scan rate of 10 °C min^{-1}. The linear sweep voltammetry (LSV) and cyclic voltammetry (CV) were characterized using CHI 760 electrochemical analyzer for obtaining the voltage window of the electrolyte. The sample codes are SPE1, SPE2, SPE3, SPE4, SPE5, and SPE6 for blend solid polymer electrolyte films with $\ddot{O}/Na^+ = 0, 2, 4, 6, 8, 10$ of $NaPF_6$ respectively.

Results and discussions

X-ray diffraction analysis

XRD is an important tool to investigate about the complex formation and change in peak position, peak intensity provides necessary information that helps us to understand the role played by salt in the blend polymer electrolyte (BPE). Figure 3 depicts the XRD diffractograms of PEO-PVP blend with different stoichiometric salt content ($\ddot{O}/Na^+ = 2, 4, 6, 8, 10$) in the 2 theta range 10 to 60°. $NaPF_6$ exhibits sharp and intense diffraction peaks near 20, 22, 32, and 44° along with two minor peaks near 32°. The absence of any sharp salt-associated peak indicates the complete dissociation of the salt. The absence of any peak associated with salt suggests the complete dissociation of the salt. All SPE shows an almost identical pattern with two crystalline peaks of PEO at 19 and 23° with some additional peaks on the addition of salt which indicates the complex formation. The additional peaks that are not of pure PEO and pure $NaPF_6$ may be due to some sort of a long-range order set by the presence of ion multiplets (as Na_2X^+, NaX_2^-, etc.) [48, 60, 61]. These two peaks at 19 and 23° are associated with the (120) and (112/032) plane, respectively. The shift in peak position confirms that the polymer blend structure is modified after addition of salt ($\ddot{O}/Na^+ = 2, 4, 6, 8, 10$), and it evidences that salt plays an effective role in altering the structure of blend polymer matrix. The reduction of peak intensity (at 19 and 23°) indicates the
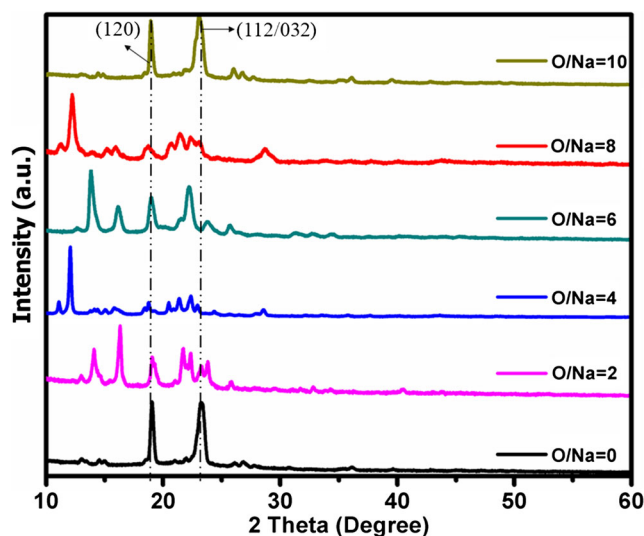

Fig. 3 XRD diffractograms for PEO-PVP + $NaPF_6$ ($\ddot{O}/Na^+ = 2, 4, 6, 8, 10$)

lowering of the crystallinity which evidences the enhancement of amorphous content owing to the cation coordination with the electron rich group of PEO/PVP. The small peaks at 13° and a broad peak near 21° are associated with the amorphous nature of PVP. The absence of any sharp peak on high salt content evidences the presence of amorphous content. This results in enhancement of ionic conductivity and may be due to improved flexibility associated with the amorphous phase and faster segmental motion of the polymer chains.

For $\ddot{O}/Na^+ = 8$, a broad hump with decreased intensity as compared to $\ddot{O}/Na^+ = 10$ is observed between 12 to 25° owing to the interaction between the cation and polymer. Thus, with the addition of salt $\ddot{O}/Na^+ = 4$, some new peaks are generated which may be due to the incomplete dissociation of the salt in the blend polymer electrolyte matrix. Few, minor peaks near 21° may be attributed to the insufficient interaction between the polymer matrix and salt that leads to ion association. Also, some peak shows splitting that is attributed to the semi-crystalline (partially crystalline-partly amorphous) nature of the solid polymer electrolyte. This needs to be validated further by more evidence as discussed in the next section.

When different salt content is added to the polymer blend, then, the peaks at 19 and a 23° shift toward the lower angle side. This indicates the increase of interlayer spacing (d-spacing) and the interchain separation (R), which reveals the complexation on the addition of salt and enhancement in amorphous content as shown in Table 1. The d-spacing between the diffraction planes was obtained using the Bragg's formula $2dsin\theta = n\lambda$ and interchain separation (R) using the equation $R = 5\lambda/8sin\theta$ [62]. As anion is going to be coordinated with the polymer backbone while cation with the electron rich group, this overall disrupts the ordering of the chains and this directly supports the enhancement of the amorphous content. This weakens the covalent bonding in between the polymer chains and cation get more free volume for migration. The

Table 1 Values of 2θ (degree), d-spacing (Å), and R (Å) of PEO-PVP + NaPF$_6$ (Ö/Na$^+$ = 2, 4, 6, 8, 10) for (120) diffraction peak

Sample	2θ (degree)	d-spacing (Å)	R (Å)
SPE 1	19.03	4.66	5.82
SPE 2	19.03	4.66	5.82
SPE 3	18.78	4.71	5.89
SPE 4	18.92	4.68	5.85
SPE 5	18.70	4.73	5.92
SPE 6	18.91	4.68	5.85

highest in both interlayer spacing (d-spacing) and the interchain separation (R) was for the SPE 5 (Ö/Na$^+$ = 8), and this suggests that the electric properties will be superior for this salt content due to high structure disorder.

FESEM analysis

The ionic transport in the solid polymer electrolyte is associated with the homogeneity of the electrolyte film, FESEM is performed to get more insights of the role played by salt in the blend polymer matrix.

Figure 4 depicts the FESEM micrographs of the pure PEO, PEO-PVP blend, and SPE 5 with composition [PEO-PVP + NaPF$_6$ (Ö/Na$^+$ = 8)] and elemental mapping of Na, P, and F in the SPE 5 system. The micrograph of pure PEO shows a rough surface with micro-cracks which is a characteristic nature of pure PEO (Fig. 4a) and is attributed to the semi-crystalline nature of the PEO. Addition of PVP in the pure PEO leads to blending and surface modification occurs as shown in Fig. 4b. This surface modification confirms the suitable interactions between both polymers. This change in the surface morphology is an indication of the reduction of crystallinity, and hence, the enhanced amorphous content. A smooth and homogenous surface morphology is evidence of fast ion transport in solid-state ionic conductor. Further, the addition of salt in the polymer blend smoothens the surface which reveals the disruption of the crystalline phase (Fig. 4c). This enhancement in the amorphous content of the polymer salt complex will facilitate the fast ion transport. Another remarkable point to be noted is that the smoothening of the surface also increases the solid polymer electrolyte film flexibility which is desirable in the field of solid-state ionic conductors. The inset of Fig. 4c displays the EDX spectra of Na, P, and F atoms which confirm their presence in the polymer salt matrix. Furthermore, the elemental mapping is implemented for imagining the Na, P, and F atoms (Fig. 4d). The uniform distribution of Na, P, and F in the entire micrograph suggests the complete dissociation of the salt; hence, the complex formation is evidenced. The smoothened surface morphology may be reflected in the enhanced electrochemical properties as explained in the upcoming section.

FTIR analysis

FTIR spectral analysis is a powerful tool to explore the molecular interaction, modification of chemical bonding in polymer electrolyte on the addition of salt [63]. Figure 5 depicts the FTIR absorption bands of PEO-PVP and PEO-PVP + NaPF$_6$ (Ö/Na$^+$ = 2, 4, 6, 8, 10) in the wave number region 600–3000 cm^{-1}, and the fingerprint region is shown by the dotted line.

The characteristics vibrations bands of PEO and PVP are noticed clearly in the PEO-PVP blend. The C-O stretching vibration located at 953 cm^{-1} is associated with PEO with some CH$_2$ rocking asymmetric vibration. The band located at 1117 cm^{-1} is attributed to the asymmetric C-O-C stretching and is a characteristic band of PEO. The vibration bands observed at 1282, 1348, and 1461 cm^{-1} are assigned to CH$_2$ asymmetric twisting, CH$_2$ bending of PEO, and CH$_2$ wagging, respectively. Two fundamental characteristic bands of PEO at 2882 cm^{-1} and near 2900 cm^{-1} correspond to the symmetric C-H and asymmetric C-H stretching, respectively [57]. The band located at 845 cm^{-1} is owing to the CH$_2$ rocking mode of PVP with a little bit of contribution from the C–O stretching mode of host polymer PEO. The C–C bending mode of vibration appears on the addition of the salt in polymer blend at 1078 cm^{-1}. The absorption band located near 1461 cm^{-1} belongs to the CH$_2$ wagging of PVP. Furthermore, PVP presence is verified by the location of two strong absorption bands at 1348 and 1687 cm^{-1} which corresponds to the C-N stretching and C=O stretching, respectively [56, 64] (Table 2).

In the present system, two interactions are possible for the cation, with (i) the electron-rich ether group of PEO and (ii) C=O of PVP. When salt is added to the polymer blend then it will approach the suitable coordinating site and will alter the environment of the polymer chain. From Fig. 5, it is clearly visible that the C=O shows minor shift and decrease of intensity in peak position. The C-O-C stretching vibration band of PEO shows peak splitting in addition to salt in symmetric and asymmetric C-O-C stretching. Also, the shift in the wave number is noticeable, which provides us strong evidence that the cation is going to coordinate with the electron-rich ether group of PEO.

Polymer-ion interaction

The addition of salt in the polymer blend alters the peak position, intensity, and peak shape which demonstrate that the polymer salt complex formation occurs (Fig. 6). This provides evidence of disruption of the polymer chains arrangement and transition from the crystalline to amorphous region. Also, with the increase of the salt loading in the blend PEO-PVP matrix, the C-O-C stretching (amorphous) mode located at 1100 cm^{-1}
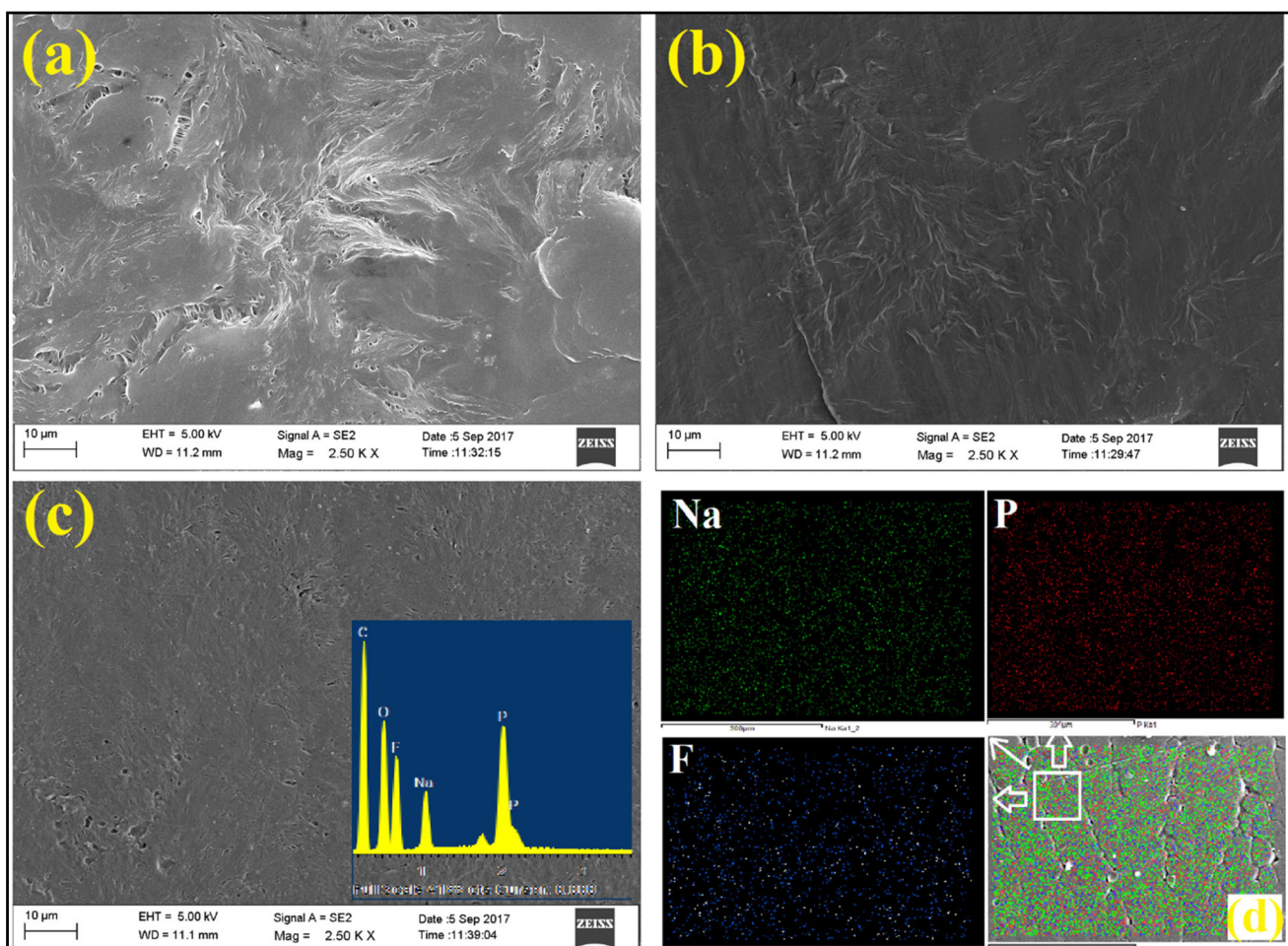
Fig. 4 FESEM micrographs of **a** pure PEO, **b** PEO-PVP blend, **c** SPE 5; PEO-PVP + NaPF$_6$ (Ö/Na$^+$ = 8) (inset shows EDX spectra), and **d** elemental mapping of Na (green dot), P (red dot), and F (blue dot) for SPE 5

and C-H stretching mode 2850–2950 cm^{-1} depicts suppression and broadening in the mode. This suppression and broadening of bands reveal the structural modification which alters the ordered arrangement and leads to reconstructions of molecular structures. It can be concluded from the above investigation that the observed shift in the positions and change in peak intensity of vibration bands suggest that the complex formation occurs on addition of salt. This is further confirmed by the impedance and the transport studies.

Ion-ion interaction

The important investigation that leads to better understanding of complex formation is the ion-ion interaction which will be examined by the anion vibration mode (PF$_6^-$). The reason behind the investigation centered toward anion mode is that cation (Na$^+$) is IR inactive. Since the envelope of PF$_6$ anion seems asymmetric, deconvolution of the corresponding peak is done using the Voigt Area function (in the Peak Fit Software) to examine the free anion (PF$_6^-$) and ion pair (Na$^+$———PF$_6^-$) contribution in wave number region ~800–900 cm^{-1}.

(Fig. 7a–e). Also, the baseline correction was done prior to deconvolution. It can be noticed from Fig. 7 that addition of salt in the polymer blend leads to change in peak intensity and asymmetry starts appearing. The symmetry of anion is reduced from $O_h \rightarrow C_3$ after interaction of cation [65, 66]. The deconvolution pattern gives two types of vibration mode due to asymmetry, one at the lower wave number side is attributed to "free anion" vibration (PF$_6^-$), while at the higher wave number side to the "ion pairs" mode (Na$^+$—PF$_6^-$) [67]. A quantitative estimation of the fraction of free anion and ion pair was estimated from the area of deconvoluted peaks assigned to particular ions using following Eq. 3:

$$
\begin{cases}
\text{The fraction of the free anion } (\%) = \dfrac{A_{free}}{A_{free} + A_{pair}} \\
\qquad\qquad and \\
\text{Fraction of ion pair } (\%) = \dfrac{A_{pair}}{A_{free} + A_{pair}}
\end{cases}
\tag{3}
$$

Here, A$_{free}$ is the area representing free ion peak and A$_{pair}$ area of the peak representing ion pair peak.
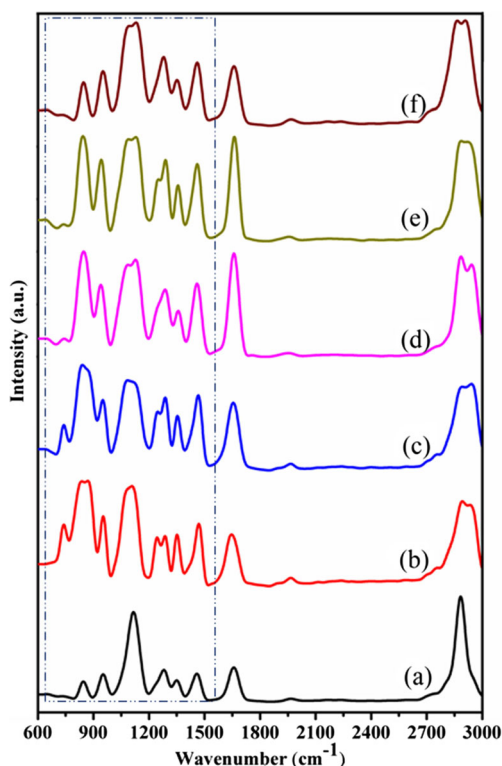
Fig. 5 FTIR absorbance spectra in the wave number range 600–3000 cm^{-1}, for PEO-PVP + NaPF$_6$ ($\ddot{O}$/Na$^+$), **a** 0, **b** 2, **c** 4, **d** 6, **e** 8, and **f** 10

A relative comparison of estimated corresponding free ion area and ion pair area is summarized in Table 3. As ion transport in polymer electrolyte is linked with polymer flexibility that is influenced by cation coordination and a number of free charge carriers, a fraction of free ions and ion pairs affect the ion transport. It is observed from Table 3 that free ion contribution increases with salt concentration, and the highest number of free ion carriers are generated for an optimum concentration which evidences the highest ionic conductivity, as shown later. This confirms that the complete salt dissociation achieved for an optimum concentration (Fig. 7f) and corresponding to which ion pair exhibits a minimum. Further, a decrease in free ion area is responsible for the decrease of ionic conductivity which will be elaborated in the following section.

Electrochemical analysis

Impedance analysis

The characteristic parameter of a solid polymer electrolyte is the ionic conductivity, and it must be analogous to the existing technology consisting of the plasticized liquid polymer electrolyte. The impedance analysis of the SPE films has been carried out by sandwiching them between two stainless steel (SS) discs which act as blocking electrodes for cation/anion under an applied electric field. The cell assembly is shown in

the inset of Fig. 8a. The impedance plot for various salt concentrations is shown in Fig. 8a. The log-log presentation of impedance plots is chosen over the traditional plot for better clarity and comparison of the different impedance plots using single plot in a unique way. The enthusiasm behind this representation was from the superiority of log plots as elaborated by Jonscher [68, 69].

In the high-frequency region of the complex impedance plots, there is a semi-circular arc for polymer blend which indicates that the conduction is mainly due to ions. In the low-frequency region, the presence of the inclined line suggests the effect of the blocking electrodes. This is evidence of the presence of capacitive nature and absence of electronic conductivity [70, 71]. The dip in the plot associated with the minima in Z'' provides us the value of bulk resistance on the real axis. The nature of all curves is almost identical. Addition of salt in the polymer blend shifts the dip in the curve toward the lower impedance side which can be correlated with the enhancement of the ionic conductivity calculated by Eq. 1. The highest ionic conductivity was 5.92×10^{-6} S cm^{-1} obtained for sample SPE 5 which is $\ddot{O}$/Na$^+$ = 8 in the PEO-PVP blend. A two-fold conductivity enhancement was achieved at room temperature as compared to the blend polymer electrolyte. This composition of blend polymer with salt ($\ddot{O}$/Na$^+$ = 8) has been referred to as the optimum conducting composition (OCC). As the conductivity is linked to a number of charge carriers and the mobility, the addition of salt alters the polymer chain arrangement which enhances the amorphous content and cation migration becomes easier. The observed room temperature ionic conductivity in the present work is higher as compared to previously reported values [52, 56, 72]. It is also observed that the conductivity increases with the addition of salt and decreases with the further addition of salt. This decrease in conductivity may be associated with the incomplete dissociation of salt. This reduces the number of charge carriers and ion pair formation occurs as evidenced by the deconvolution of FTIR. Also, sample SPE 2 displays another maximum in electrical conductivity. Figure 8b displays the fitted impedance plot of OCC (sample 5) with an equivalent circuit using the $Z_{SimpWin}$ software. The equivalent circuit shown in inset consists of the constant phase element (Q_1) in parallel with resistance and in series with another constant phase element (Q_2).

Temperature dependence of ionic conductivity

The ionic conductivity of the prepared SPE films was measured in the temperature range of 40 to 100 °C. The ionic conductivity was highest for sample SPE 5 with composition PEO-PVP+$\ddot{O}$/Na$^+$ = 8. As temperature rises, it enhances the polymer chain flexibility which leads to faster ion mobility, and hence ionic conductivity. So, further insight toward understanding the effect of temperature, impedance was measured at

Table 2 FTIR spectral data of PEO-PVP, PEO-PVP + NaPF$_6$-based SPE films

Wave number (cm^{-1})						Band assignment
SPE 1	SPE 2	SPE 3	SPE 4	SPE 5	SPE 6	
844	832	842	844	842	844	C-O stretching in PEO/PF$_6^-$ vibration and CH$_2$ rocking of PVP
953	955	950	938	943	953	C-O stretching vibration
1117	1078/1120	1080/1120	1080/1127	1083/1130	1090/1132	Symmetric and asymmetric C-O-C stretching (amorphous)
1282	1245/1287	1242/1289	1248/1287	1242/1289	1279	CH$_2$ symmetric/ asymmetric twisting
1348	1350	1353	1360	1355	1350	CH$_2$ bending of PEO and C-N stretching of PVP
1461	1468	1466	1459	1459	1460	CH$_2$ wagging
1657	1643	1655	1660	1662	1658	C=O stretching
2882	2891	2844	2886	2880	2861	Symmetric C-H stretching
–	2948	2945	2938	2932	2911	Asymmetric C-H stretching/CH$_2$ asymmetrical vibration

a different temperature. The measured impedance plots of the SPE 5 sample at different temperatures are presented in Fig. 8c. It can be noticed from Fig. 8c that the dip in the curve shifts toward the lower impedance side which indicates the lowering of bulk resistance and hence the enhanced ionic conductivity. This enhancement in the ionic conductivity with an increase of temperature may be associated with the increased polymer chain flexibility and a number of free charge carriers.

Also, the activation of free charge carriers between the coordinating sites and the segmental motion of the polymer chains may occur due to increased free volume [72, 73]. This increased flexibility of polymer chains indicates the increase in the ion mobility which promotes the smoother ion migration.

Figure 8d depicts the variation of ionic conductivity with salt content at a different temperature. It can be concluded from Fig. 8d that the ionic conductivity increases with the
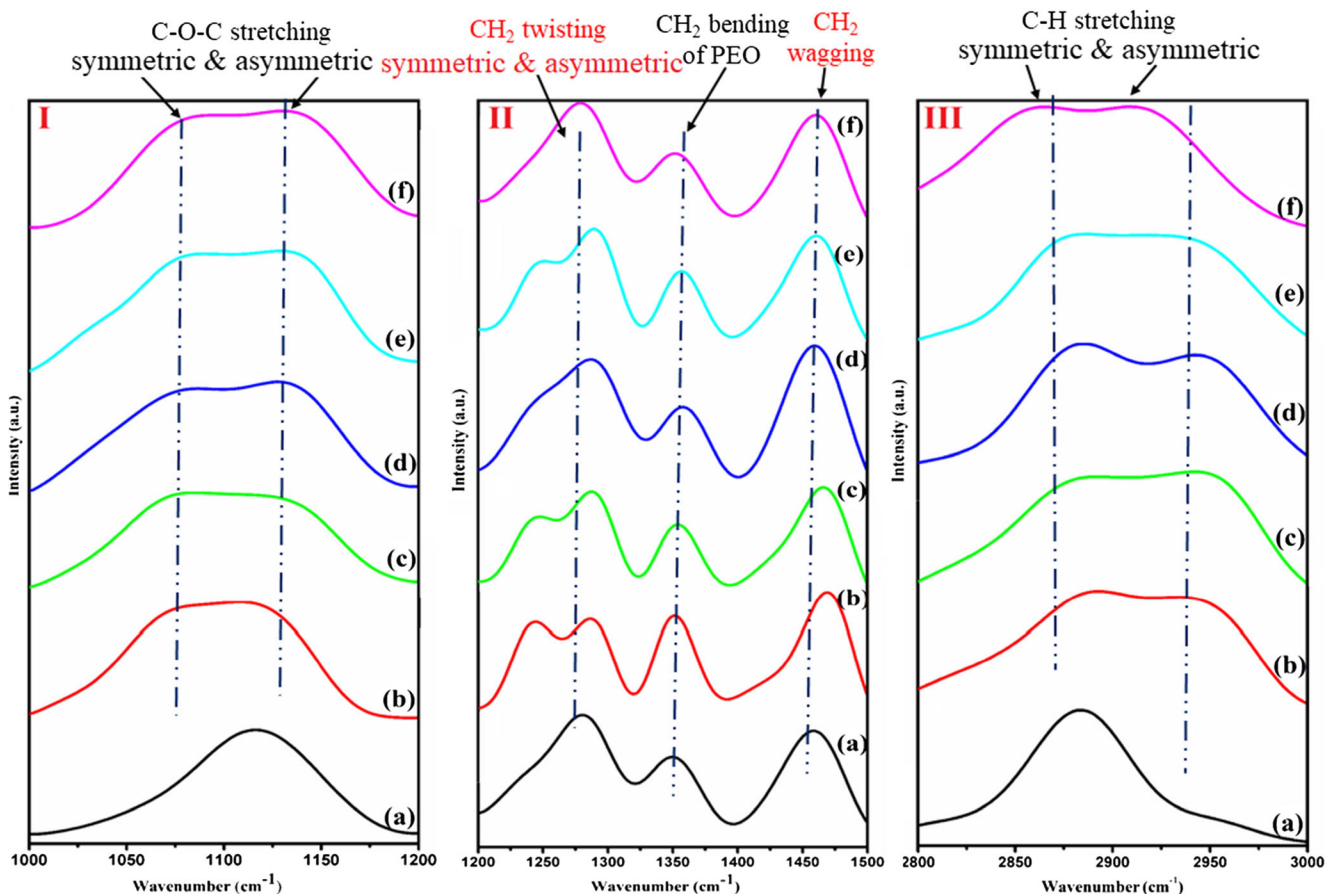

Fig. 6 FTIR spectra for PEO-PVP + NaPF$_6$ (Ö/Na$^+$) = **a** 0, **b** 2, **c** 4, **d** 6, **e** 8, **f** 10 (I) C-O-C stretching mode, (II) CH$_2$ twisting/wagging/bending mode, and (III) C-H stretching mode
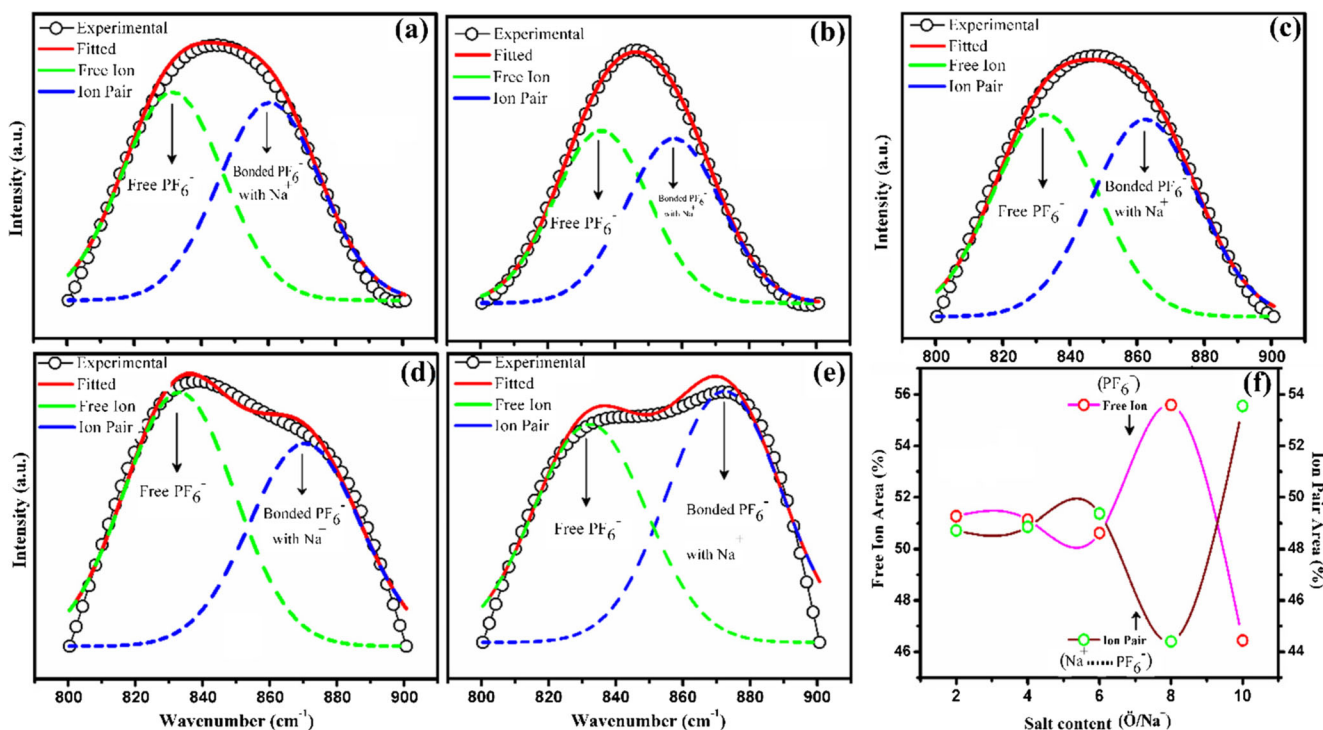
Fig. 7 Deconvolution of the PF_6^- vibration mode in the wave number range 800–900 cm^{-1} for PEO-PVP + $NaPF_6$ ($Ö/Na^+$), **a** 2, **b** 4, **c** 6, **d** 8, and **e** 10 using the Voigt area function. **f** Salt concentration dependence of free anion and ion pair area

temperature and is maximum at the highest temperature. The highest ionic conductivity achieved was 5.92×10^{-6} S cm^{-1} at 40 °C and increased to 2.46×10^{-4} S cm^{-1} at 100 °C (Table 4). A comparison of ionic conductivity for a various blend polymer matrix with different salts is represented in Table 5, and it can be concluded that the present blend polymer matrix has improved conductivity more than the other reports known from literature till date. It validates the use of synthesized BPE for application in sodium-based energy storage devices. Figure 8d displays the temperature-dependent ionic conductivity of the investigated polymer electrolyte in the temperature range of 40 to 100 °C. Here, the ionic conductivity seems to be increased with the temperature owing to the enhancement of the polymer flexibility which increases the cation (Na^+) mobility. Almost a linear variation in conductivity is observed with temperature. For the lower salt concentration ($Ö/Na^+ = 10$), only a minor increase in conductivity is observed and may be due to the availability of less number of free charge carriers. Further, the conductivity increases up to $Ö/Na^+ = 8$ and after that is followed by a decrease for the $Ö/Na^+ = 4, 6$. This may be due to the optimum value of Na w.r.t. number (8) of the polymer chain and continuous hanging of anion in the polymer chain. While for the very high salt content again conductivity increases that may be due to the effective role played by anion along with cation in charge transport Further increasing the salt concentration lowers trend of electrical conductivity due to strong ion pairing of Na/PF_6.

The enhancement of the ionic conductivity is attributed to the salt dissociation owing to the polymer-ion and ion-ion interaction. The salt dissociation results in the release of a free number of ions and is highest for the content which shows conductivity maxima as evidenced by the FTIR deconvolution. The first maxima is associated with the cation migration as an anion is hanged to the polymer backbone. So, the segmental

Table 3 The peak position of deconvoluted free ion and ion pair peak of SPE films

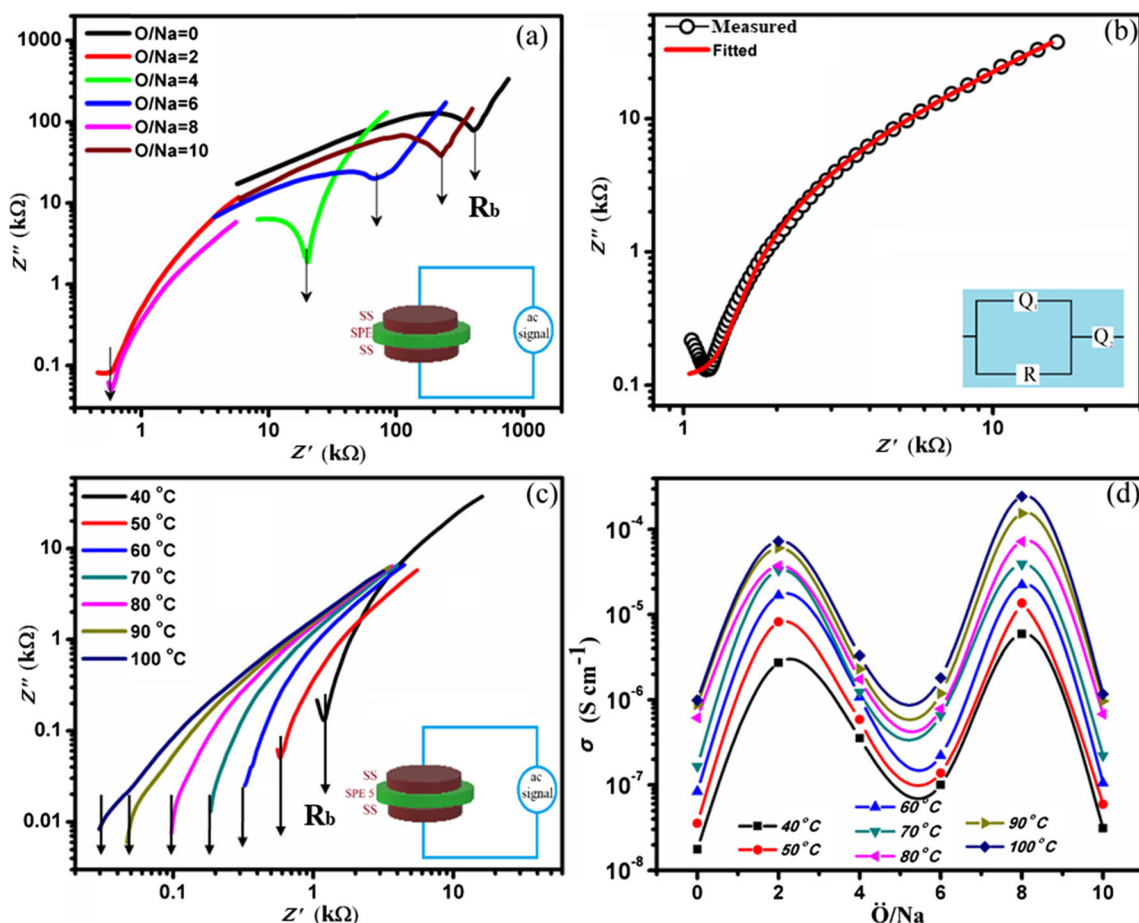| Sample code	Free ion		Ion pair		Corr. coff. (r^2)
	Area (%)	Wave number (cm^{-1})	Area (%)	Wave number (cm^{-1})	
SPE 2	51.27	832	48.72	860	0.992
SPE 3	51.13	836	48.86	857	0.998
SPE 4	50.62	833	49.37	862	0.994
SPE 5	55.59	833	44.40	869	0.979
SPE 6	46.44	833	53.55	870	0.954

Fig. 8 **a** Room temperature log-log complex impedance plots for different salt concentration ($\ddot{O}/Na^+ = 2, 4, 6, 8, 10$). Inset of **a** depicts cell configuration, **b** fitting of impedance plot for SPE 5. Inset of **b** depicts fitted circuit element, **c** log-log impedance plot of SPE 5 at different temperature (40–100 °C), and **d** variation of ionic conductivity with salt concentration ($\ddot{O}/Na^+ = 2, 4, 6, 8, 10$) at different temperatures (40–100 °C)

motion of the polymer chain plays an effective role in enhancing the ion transport. Then, another maximum is achieved at high salt content which is associated with the anion migration. As at high salt content number of both cation and anion increase, the former one gets trapped via the ion cross-linking formation, while anion stays out the cation path due to high concentration. This results in the disorder in the polymer matrix and anion starts migrating via the polymer backbone having CH_2 group. Since anion bears a larger size and mass, so, it demonstrates

comparative conductivity with the cation. Further, explanation of the conductivity maxima is explained by the transport parameter measurement and the mechanism termed as two percolation peak mechanism in the upcoming section.

Conductivity stability and ion transference number

To highlight the suitability of solid polymer electrolyte at high temperature (100 °C), conductivity monitoring is done for the

Table 4 Conductivity variation with temperature for different salt contents

Sample code Temperature	SPE 1	SPE 2	SPE 3	SPE 4	SPE 5	SPE 6
40 °C	1.77×10^{-8}	2.74×10^{-6}	3.55×10^{-7}	1.01×10^{-7}	5.92×10^{-6}	3.11×10^{-8}
50 °C	3.54×10^{-8}	8.19×10^{-6}	5.87×10^{-7}	1.38×10^{-7}	1.36×10^{-5}	5.94×10^{-8}
60 °C	8.40×10^{-8}	1.67×10^{-5}	1.08×10^{-6}	2.21×10^{-7}	2.24×10^{-5}	1.05×10^{-7}
70 °C	1.66×10^{-7}	3.32×10^{-5}	1.23×10^{-6}	6.56×10^{-7}	3.92×10^{-5}	2.22×10^{-7}
80 °C	6.15×10^{-7}	3.74×10^{-5}	1.74×10^{-6}	6.43×10^{-7}	7.22×10^{-5}	6.79×10^{-7}
90 °C	8.82×10^{-7}	6.05×10^{-5}	2.31×10^{-6}	1.19×10^{-6}	1.55×10^{-4}	9.69×10^{-7}
100 °C	9.89×10^{-7}	7.29×10^{-5}	3.29×10^{-6}	1.81×10^{-6}	2.46×10^{-4}	1.17×10^{-6}

Table 5 Comparison of the ionic conductivity of various sodium and lithium salts

Polymers	Salt	Ionic conductivity	Temperature	Reference
PEO-PEMA	$NaClO_4$	6.77×10^{-7} S cm^{-1}	30 °C	[74]
PEO-PVP	$NaIO_4$	1.56×10^{-7} S cm^{-1}	RT	[75]
PEO-PVP	NaF	1.19×10^{-7} S cm^{-1}	RT	[46]
PVC-PEMA	$NaIO_4$	10^{-8} S cm^{-1}	RT	[76]
PEO-PVP	$LiClO_4$	3.77×10^{-6} S cm^{-1}	40 °C	[56]
PEO-PVP	NaBr	1.90×10^{-6} S cm^{-1}	RT	[54]
PEO-PVP	$NaPF_6$	5.92×10^{-6} S cm^{-1}	40 °C	Our work
PEO-PVP	$NaPF_6$	2.46×10^{-4} S cm^{-1}	100 °C	Our work

optimized PEO-PVP + $NaPF_6$ ($\ddot{O}$/Na$^+$ = 8) highly conducting system. The conductivity can still be maintained stably up to 160 h (approx. 7 days) as shown in Fig. 9a. The above advantages of the prepared solid polymer electrolyte can serve as a suitable candidate for long-term safe solid-state sodium ion battery.

The fraction of current carried by ions in the prepared SPE is important to analyze. Now, the ion transference number measurement was performed using Wagner's DC polarization technique. As SPE 5 system has optimum conductivity for practical application in energy storage devices, we performed the ion transference number measurement for the PEO-PVP + $NaPF_6$ ($\ddot{O}$/Na$^+$ = 8) system with an applied dc bias ~50 mV across the configuration SS|SPE 5|SS (Fig. 9b). The plot shows initially high current (i_t) and drops sharply with an increase of time followed by a steady state associated with current i_e. The former one is a contribution from both ions and electrons while the later one is an only electronic current contribution. For the perfect ionic conductor, the value of ion transference number is supposed to be unity. We have measured the ion transference number (t_{ion}) for the highest conducting sample and is found to be 0.997 using Eq. 2.

On the application of electric field on the cell configuration SS|SPE|SS, both ions and electrons respond to the applied field. The stainless steel (SS) electrodes prevent the ion flow to an external circuit by creating a zone of mobile ions on the electrode/electrolyte interface. Then, further ion migration is

constrained by this zone; after some time, it dominates over the applied field and concentration polarization is achieved. Now, the current starts decaying due to the balance of drifted ions and diffused ions. As a result of this, a concentration polarization zone formed at electrode/electrolyte interface increases the interfacial resistance and ionic current is blocked now while permitting electronic current. So, after some time, only electronic current is dominating. This value is close to value of perfect ionic conductor, and it concludes that the present system is ion dominating with most of the charge transfer (~ 99%) by ions with negligible electron contribution [77, 78].

Thermal activation energy measurement

Another important parameter to investigate the ion migration is activation energy (E_a). It depicts the energy associated with the defect formation and the ion migration simultaneously. The value of activation energy basically tells about the favorable environment and the conditions for the ion migration for smoother ion transport. The high value of activation energy may be due to the requirement of high energy for ion migration [79, 80]. Now, all the plots were fitted with the Arrhenius equation to obtain the value of activation energy (E_a) from the slope of linear portion (Fig. 10a). From the plot, it can be concluded that all SPE shows perfect agreement with the Arrhenius equation (the solid red line is the fitted equation). From the results, it was obtained that the SPE system with the

Fig. 9 **a** Conductivity stability of the PEO-PVP + $NaPF_6$ ($\ddot{O}$/Na$^+$ = 8) at a high temperature of 100 °C and **b** variation of current with respect to time across the cell; SS|SPE 5|SS
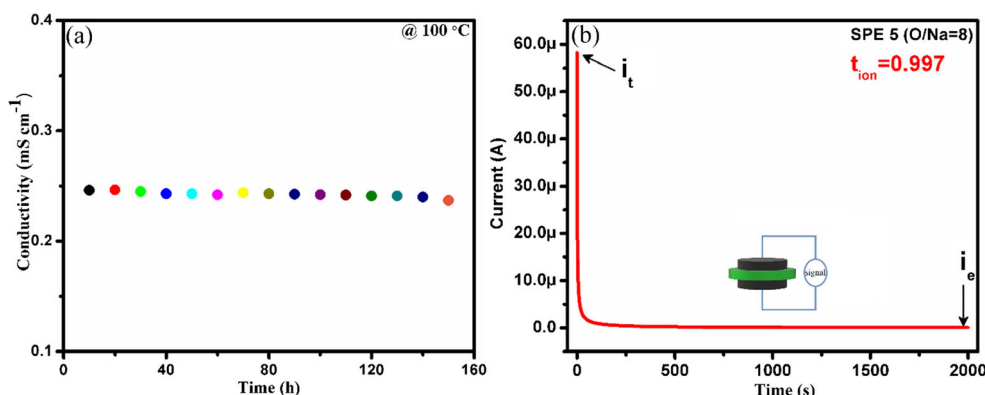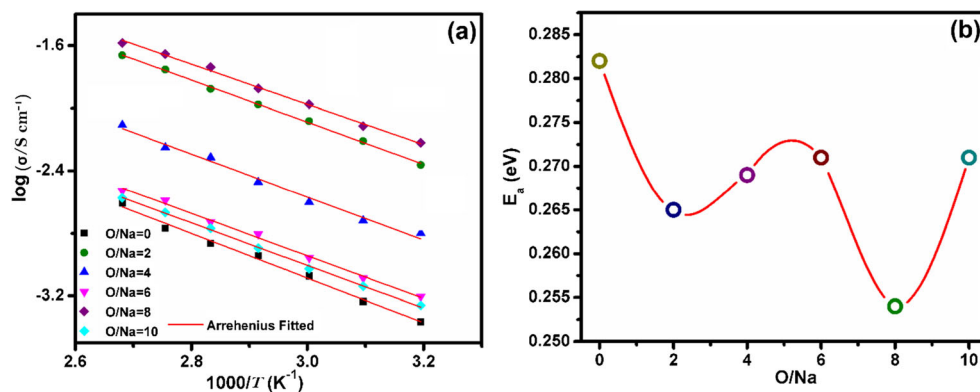
Fig. 10 a Arrhenius plot and **b** activation energy plots for PEO-PVP blend polymer electrolyte with different salt concentrations ($\ddot{\text{O}}$/Na$^+$ = 2, 4, 6, 8, 10)

highest conductivity (SPE 5) sample has conducting pathways of the lowest activation energy as compared to other blend polymer salt complexed electrolyte (Fig. 10b). So, ionic conductivity depends on the activation energy of the free ions directly and the smaller the activation energy, the smoother the cation migration. This lowering in the activation energy is owing to the increase of flexibility of polymer chains for this concentration which makes a favorable conductive path for the ions. All SPE shows the value of activation energy in the range of 0.2 to 0.3 eV and is in desirable range for the fast solid-state ionic conductor. Another point to be noted here is that the activation energy values are in absolute agreement with the free ion area obtained from FTIR and the impedance study.

Transport parameters

The desirable property of a solid polymer electrolyte is high ionic conductivity (σ) which is directly linked with number density (n), mobility (μ) of charge carriers, viscosity (η), and diffusion coefficient (D) for any plastic separator stands for electrolyte cum separator. As the electrical conductivity value of solid polymer electrolyte films is directly dependent on a number of free charge carriers and mobility ($\sigma = nq\mu$), the FTIR spectroscopy was used to evaluate the parameters using the equation reported somewhere [81]. FTIR deconvolution was done to determine the percentage area of free ion and ion pair and the areas are plotted as a function of salt content (Fig. 7d). Figure 11 displays the variation of mobility (μ), viscosity (η), and diffusion coefficient (D) of charge carriers against the different salt content. It reveals the one-to-one correspondence between charge carrier mobility (μ) and diffusion coefficient (D). Both the mobility and diffusion coefficient of charge carriers increases with addition of salt. The maximum for both was achieved for the optimum conductivity value (PEO-PVP + NaPF$_6$ ($\ddot{\text{O}}$/Na$^+$ = 8)). Also, viscosity of polymer chains influences the charge migration so it was investigated and follows inverse trend as of mobility or conductivity. The maxima in the conductivity or mobility is associated with minima in the viscosity. This concludes that the viscosity of polymer chain reduces with addition of salt and leads to faster ion migration [82]. This result is also in good agreement with the associated FTIR ion-ion interaction and conductivity studies.

Differential scanning calorimetric (DSC) analysis

In case of polymer electrolytes, various phase transitions occur with temperature and provide crucial information to explain the enhancement of the electrical properties. So, DSC was performed (Fig. 12) to measure the glass transition temperature (T_g), melting temperature (T_m), and crystallinity (X_c) and their variation with salt content is shown in Table 6. It needs to be mentioned here that the glass transition is linked to the polymer chain flexibility and ion mobility. The low value of T_g indicates faster ionic transport due to the increased polymer chain segmental motion. The blend polymer electrolyte shows T_g about − 69.02 °C and the addition of salt in the polymer blend evidence the shift toward lower temperature. Further addition of salt in the blend polymer electrolyte demonstrates little change in the T_g with the lowest value for the SPE 5 (O/Na = 8) followed by the SPE 2 (O/Na = 2). The shift on the T_g is attributed to the reduction of the covalent bonding between the polymer chains due to ion penetration. The almost same trend is followed by the peak associated with melting temperature (T_m) where polymer gets melted. The shift of peak toward lower temperature indicates the increased ionic conductivity and both T_g and T_m supports this approach [83, 84].

The crystallinity was calculated using Eq. 3 and it shows the crystallinity minima for the SPE 2 system. Although the crystallinity is lowest for the blend polymer electrolyte with O/Na = 2, conductivity was highest for the O/Na = 8-based polymer electrolyte. The crystallinity with the addition of optimum salt content is much smaller in comparison to the blend polymer electrolyte (without salt). This indicates that the addition of salt disrupts the crystalline arrangement of the polymer chain by eliminating the covalent bonding of the polymer chains (Na$^+$—O- and PF$_6^-$——H$_2$C-). So, the enhanced amorphous content is achieved, which favors the faster ion migration.
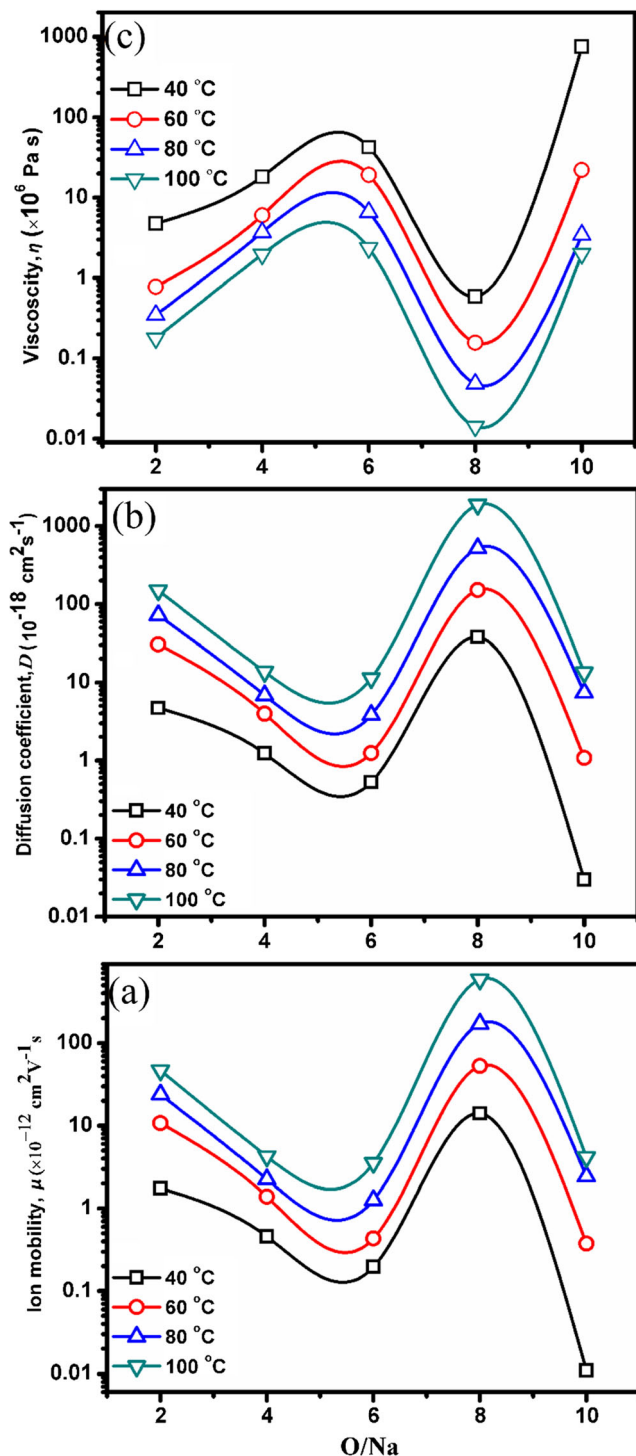
Fig. 11 The plot in a variation of **a** mobility (μ) of charge carriers, **b** viscosity (η), and **c** diffusion coefficient (D) against the salt content

The enhanced amorphous content is also linked to the increased free volume that provides the smoother path to the cation. It can be concluded that the lowering of the T_g and T_m value along with crystallinity reduction with the addition of salt provides sufficient evidence for the enhancement in the conductivity.

Atomic force microscope (AFM) analysis

AFM has been used to study the morphological changes after addition of salt in blend polymer electrolyte (BPE). The two-dimensional image of the polymer blend (without salt) and polymer blend with $\ddot{O}/Na^+ = 8$ having optimum ionic conductivity are shown in Fig. 13. From Fig. 13a, b, it is observed that the average roughness value of the polymer blend is about 80 nm. The surface roughness factor plays an important role in the enhancement of ionic conductivity and linked with amorphous content. When salt is added to the polymer blend, then, the severe surface modification indicates that the salt plays an active role as shown in Fig. 13c, d. Addition of salt reduces the crystallinity of the blend polymer electrolyte and makes the surface smoother which is favorable for faster ion conduction [85]. Now, the surface roughness value increases to about 130 nm. This increase in roughness value indicates the complex formation of a polymer blend with salt and amorphous content improved [86]. This increase in the roughness parameter and amorphous content is responsible for the enhancement of ionic conductivity and promotes ion migration. It can be concluded that the addition of salt modifies the structure of the blend polymer electrolyte (BPE) and is in close agreement with the XRD, FESEM and Impedance study.

Thermo-gravimetric analysis (TGA)

Thermal stability of a battery device is important to avoid the material decomposition and explosion during cell operation. So, the thermal stability was investigated by TGA to check the safety window of solid polymer electrolyte [87]. The thermograms of PEO-PVP blend and PEO-PVC + NaPF$_6$ with $\ddot{O}/Na^+ = 2$ and 8 are plotted in Fig. 14 and the thermogram is divided into three regions for a better understanding of various decomposition stages.

In *region 1*, initially a small weight loss is observed at 60–80 °C and that may be due to the evaporation of the solvent and the moisture content during loading of the sample [62, 88]. PEO-PVP blend with both salt stoichiometric ratio shows identical thermal stability.

Now, in *region 2*, PEO-PVP blend shows a small weight loss of approx. 15%. In PEO-PVP blend without salt, one step loss is observed while after addition of salt one additional step is clearly visible. This multi-step process confirms that the present system is BPE [89]. Addition of salt alters the thermal stability and for higher salt content ($\ddot{O}/Na^+ = 2$) more weight loss is observed as compared to $\ddot{O}/Na^+ = 8$. Here, salt is acting as an opponent and reduce thermal stability of overall solid polymer electrolyte. This may be due to the increased flexibility of polymer chains. Now, less energy is required to disrupt the bonding and reduction of thermal resistance leads to decomposition at a lower temperature. However, the
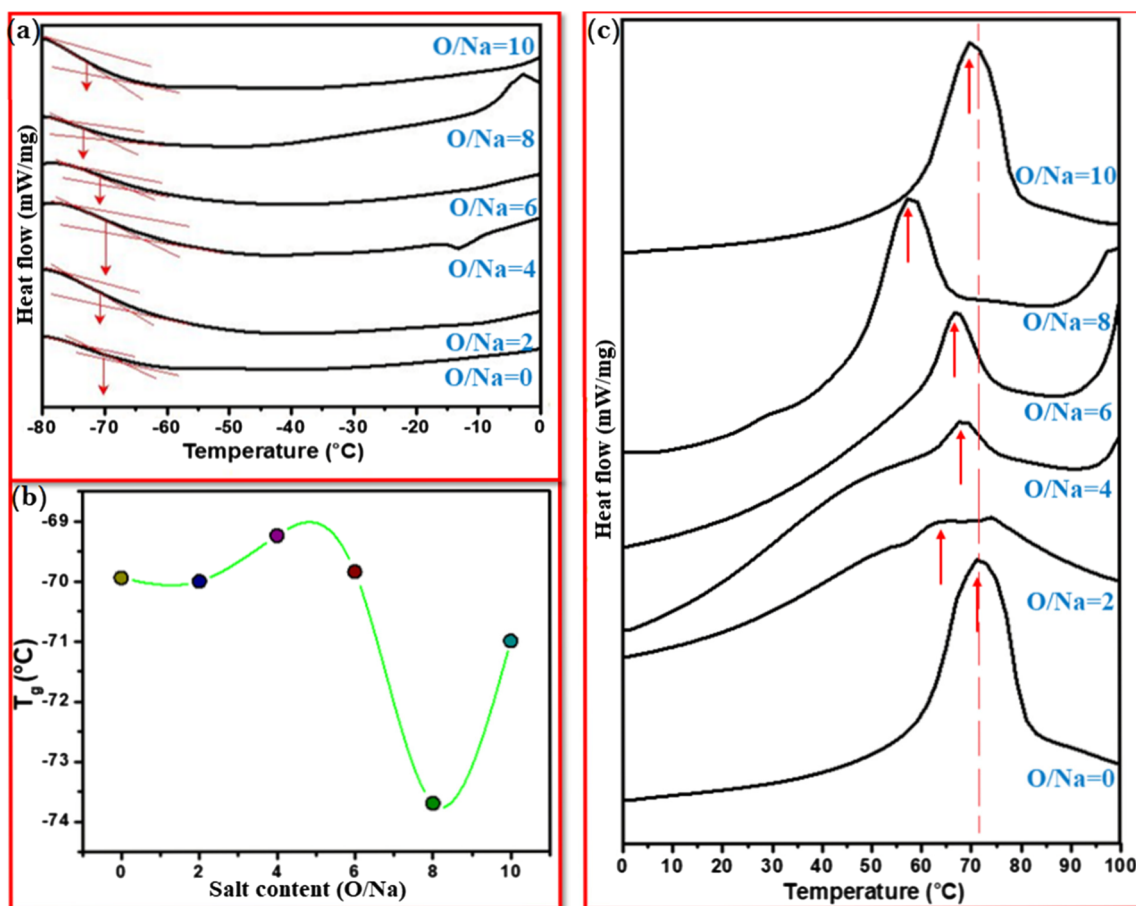
Fig. 12 DSC thermograms for the solid polymer electrolytes, **a** DSC trace, **b** variation of glass transition temperature against salt content, and **c** variation of the melting peak. Approximate O/Na ratio is also given for each sample

addition of salt shifts the graph toward lower temperature only up to 70–80 °C. The rapid weight loss in various steps confirms the degradation of the sample beyond 300 °C. In *region 3*, the polymer matrix constituents such as a polymer, salt start to degrade and weight loss is maximum. The solid polymer electrolyte cannot be completely decomposed even when the temperature reaches 600 °C. In case of polymers, at high temperature, two types of decomposition process are known, (i) chain de-polymerization or unzipping and (ii) random decomposition. The former one is just the release of the chains from weak link while the later one occurs via chain rupturing at

Table 6 Thermal properties of the blend polymer with different salt contents

Sample code	T_g (°C)	T_m (°C)	X_c (%)
O/Na = 0	− 69.02	71.71	49.36
O/Na = 2	− 72.03	68.21	1.29
O/Na = 4	− 70.23	67.25	2.26
O/Na = 6	− 70.42	66.89	4.72
O/Na = 8	− 77.21	59.31	5.21
O/Na = 10	− 72.89	70.78	47.56

random points. Both processes contribute to loss of mass [54]. The plateau region or almost zero loss region confirms the thermally stable up to approx. 200 °C and is enough to fulfill the demand of electrolyte in energy storage/conversion devices. Obviously, we can claim from these observations that these SPE can be operated up to 200 °C and are preferred in the SIB as its operating temperature is normally below 100 °C.

Electrochemical stability window

Electrolyte stability window (ESW) enables us to obtain the maximum operating neutral voltage range with an applied potential of the polymer electrolyte for device applications. Linear sweep voltammetry is performed to obtain the ESW in the configuration of SS/SPE5/SS at 40 and 80 °C within the voltage range of 0–5 V at a scan rate of 10 mV/s. From Fig. 15, it can be noticed that initially the current remains in steady state and then shows a sharp increase that is attributed to the electrolyte decomposition at inert electrode interface [90–92].

The voltage window is up to at least 3.5 V for the SPE 5-based system (Fig. 15a). Furthermore, the high-temperature stability (80 °C) of the SPE 5 system is investigated. From Fig. 15b, it is clearly visible that the voltage window is stable
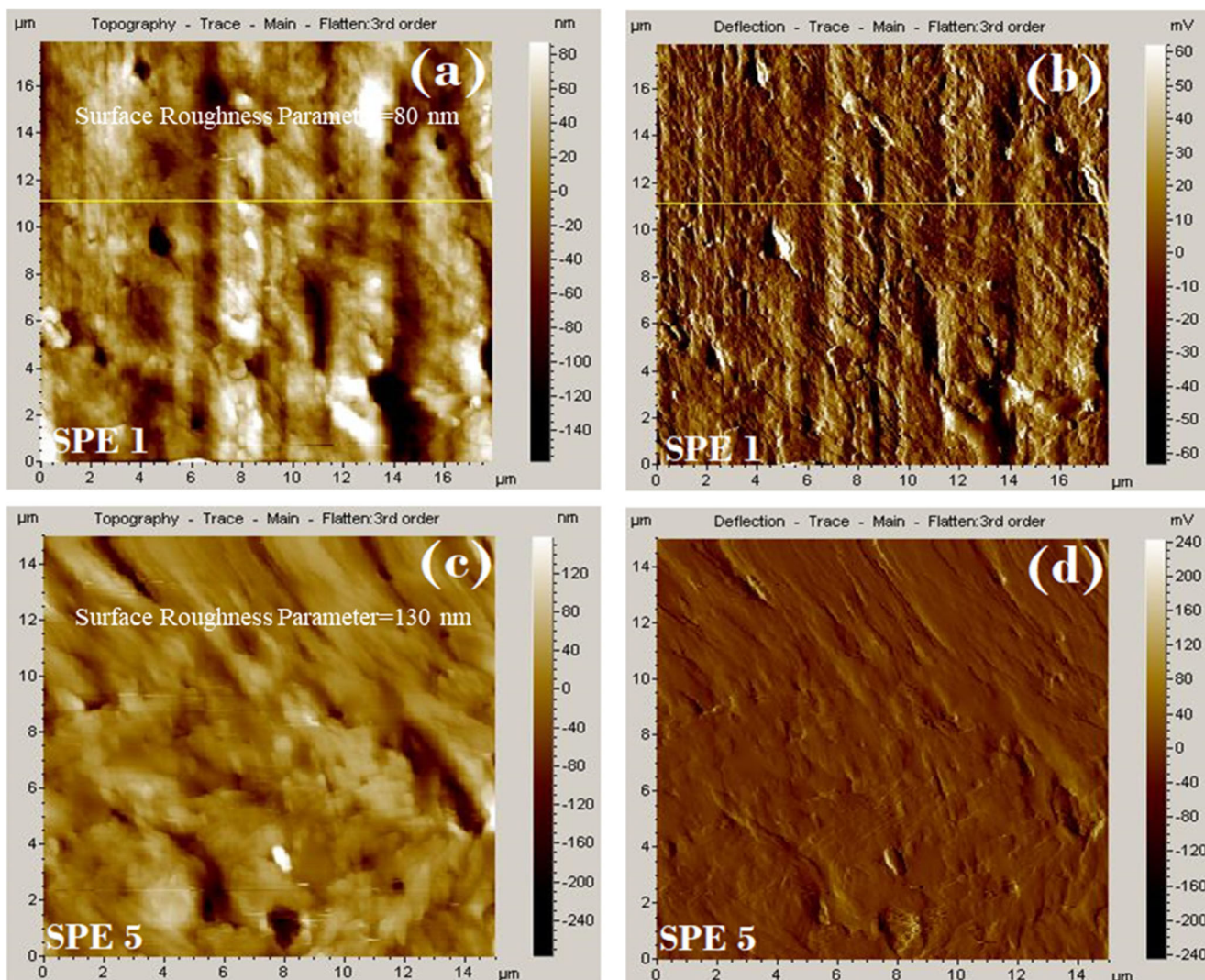
Fig. 13 Two dimensional **a** and **b** topography and deflection image of PEO-PVP and **c** and **d** Topography and deflection image of PEO-PVP + NaPF$_6$ ($\ddot{O}$/Na$^+$ = 8)

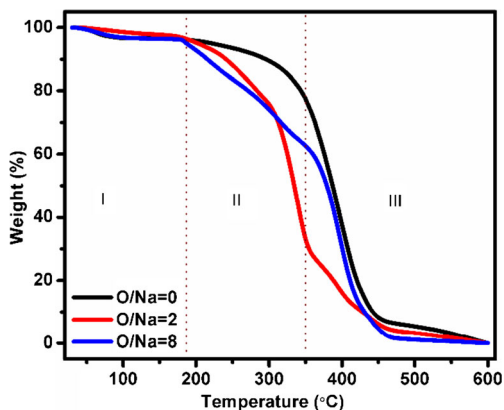up to 3.5 V which safeguards the application of prepared solid polymer electrolyte at high temperature.

Fig. 14 TGA curves of PEO-PVP blend, PEO−PVP + $\ddot{O}$/Na$^+$ = 2, and PEO-PVP+$\ddot{O}$/Na$^+$ = 8

The cyclic voltammetry (CV) study of the SPE 5 system was measured in the voltage range − 3 to 3 V with a scan rate of 10 mV/s for 5 cycles (Fig. 15c, d). The configuration for the measurement was SS/SPE 5/SS. From Fig. 15c, it can be concluded that the stability of polymer electrolyte remains even after 5 cycles and this evidences the applicability of polymer electrolyte for application in the voltage range of at least 5 V. Also, the repeatability in the curve confirms the voltage stability of the investigated system. Now, to test the high-temperature applicability of the prepared polymer electrolyte, high-temperature voltage stability (80 °C) is measured by CV. Figure 15d shows both cyclic and thermal stability of the solid polymer electrolyte. Another noteworthy point is that absence of any cathodic/anodic peak for both low and high-temperature CV curve confirms the broad stability window for the long-term application. Overall, both LSV and CV support the use of prepared polymer electrolyte with long-term cycle stability and thermal stability for the solid-state sodium ion batteries.
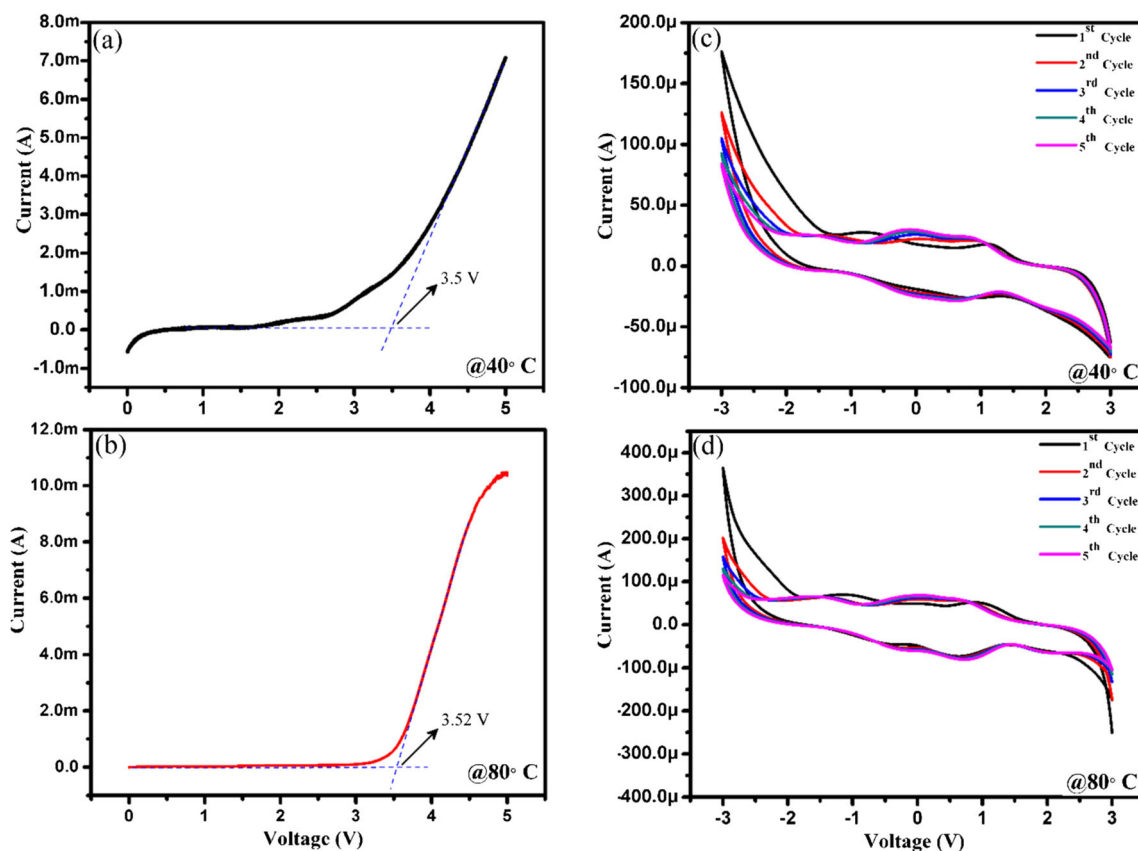
Fig. 15 Linear sweep voltammetry of SS/SPE 5/SS, **a** 40 °C, **b** 80 °C and cyclic voltammetry curves of the system SS/SPE 5/SS, **c** 40 °C, and **d** 80 °C

Two peak percolation model/mechanism

The enhancement of the ionic conductivity is further examined by proposing the model that highlights the individual role played by the polymer and the salt. This model is based on the results obtained by the FTIR, impedance study, and the transport parameters. Figure 16a–g depicts the ion transport mechanism. When the salt is added in blend polymer, various interactions occur depending on the availability of sites for interaction. Figure 16a displays the four possible interactions as a general case, (i) F of anion with the H of PEO, (ii) P of anion may interact with N of PVP, (iii) F of anion with the H of PVP, and (iv) P of anion may interact with O of PVP. Out of all four possibilities, the first and second seems to be feasible and more appropriate in the present case based on microscopic interaction among a different functional group of polymer and salt through FTIR result findings. The hydrogen bonding between the F of the anion with the H of PEO and anion interaction with the blend polymer is effective in the formation of the polymer salt complex. First of all, when the two polymers are dissolved, then, both PEO and PVP interact via the hydrogen bonding (Fig. 16b, c). This formation of the blend was also confirmed by the DSC as single glass transition temperature was observed for the present system. Now, when the salt is added to the polymer electrolyte, then, the salt gets

dissociated in the cation and anion. Now, the cation gets coordinated with the ether group of the polymer chain as evidenced by the FTIR (Fig. 16d). The anion gets coordinated with N of the PVP. This interaction alters the polymer chain arrangement and the viscosity of the chain decreases. Now, when the addition of the salt is done in the blend polymer electrolyte, then, the migration of the ion occurs via the segmental motion of the polymer chains. The salt gets coordinated with the ether group of the host polymer while anion with the polymer backbone. The formation of new coordinating sites and elimination of previous sites leads to cation transport (Fig. 16e). The sufficient sites are to participate in the ion transport. With the increase of the salt content, dissociation of the salt increases as well as a number of free charges carriers. As conductivity is linked to the number of free charge carriers, so, conductivity is enhanced and first maxima are achieved (Fig. 16e). Now, when the salt content is increased, then there arises the possibility of the ion pair formation as observed by the FTIR deconvolution and decrease of free ion area is observed. Figure 16f shows the formation of ion pairs due to the absence of sufficient cording sites for cation coordination. This restricts the salt dissociation and conductivity decreases. Now, further increase of the salt content enhances the ion transport; the ion charges carriers are anions. As now, the disorder in the polymer chain is more and number of anion

Fig. 16 Proposed mechanism, **a** four possible interaction of the salt with polymer matrix; **b**, **c** blend polymer electrolyte formation; and **c** polymer salt complex formation, and interaction at **d** optimum salt content, **e** moderate salt content, **f** high salt content, and **g** very high salt content. The bold rectangle depicts the various active species in the interaction
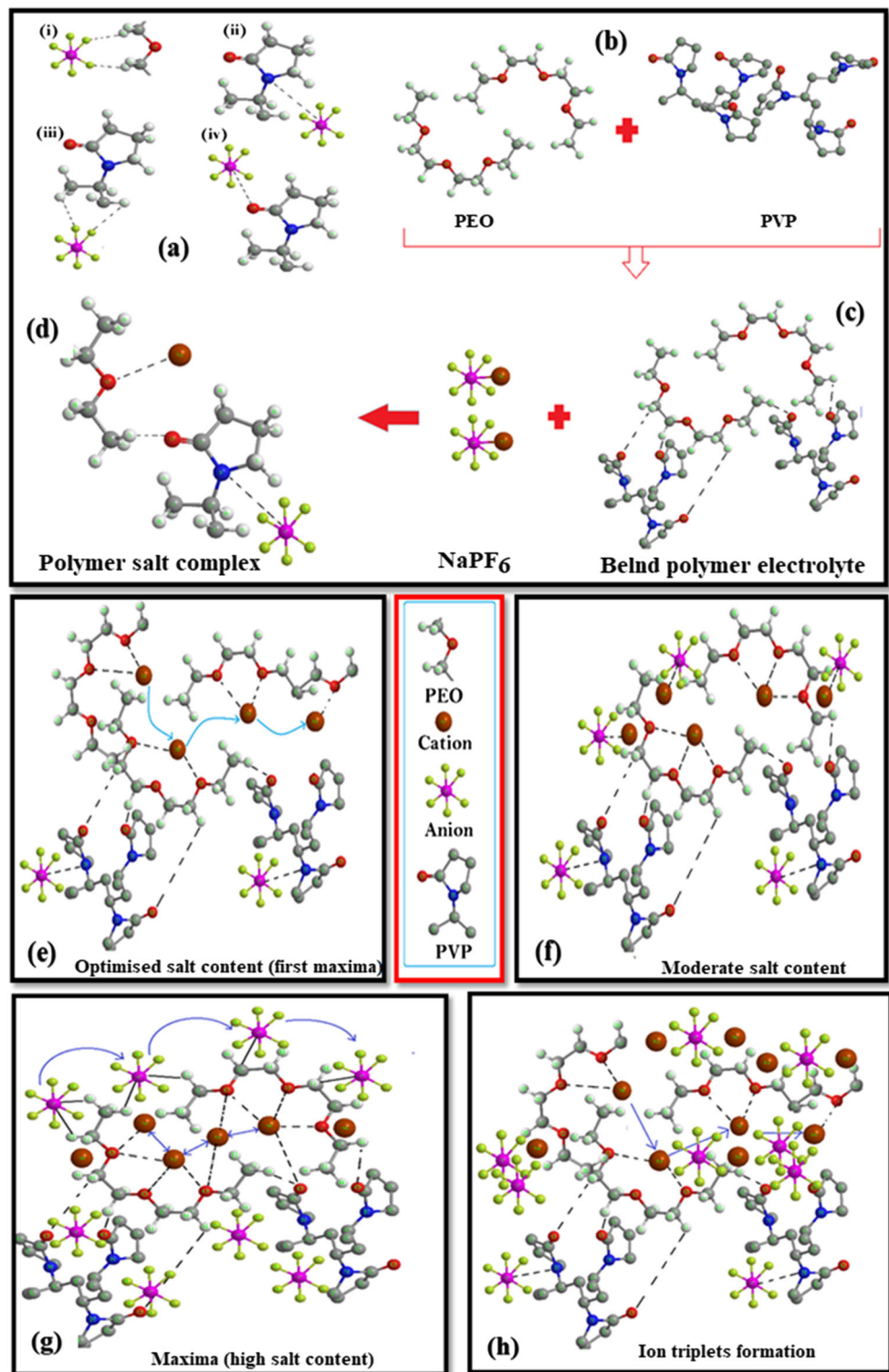
is also large. As cation is of smaller size than the anion, so, it gets trapped in between the polymer chains via the ion cross-linking that traps the cation and halts its migration. As it is well known that the anion is attached to the polymer backbone or resides outside the polymer chains, the anion starts participating in the conduction via the polymer backbone

group and second maxima is achieved (Fig. 16g). Further addition of the salt content in the blend polymer electrolyte leads to the ion-triplets formation and lowering of the conductivity is observed (Fig. 16h). Actually, at high salt content, the segmental motion is not so effective and salt dissociation is not observed.

Conclusions

The flexible and freestanding blend solid polymer electrolyte films based on PEO-PVP complexed with $NaPF_6$ were synthesized by the standard solution cast technique. The reduction of peak intensity from the XRD evidenced the increase of the amorphous content and increased interchain separation. FESEM micrograph displays the formation of the smoother surface with the addition of salt which indicates the enhanced amorphous content. AFM analysis also supports the enhancement of the amorphous content. FTIR confirmed the cation coordination with the ether group of the polymer chain and polymer salt complex formation explained in terms of the presence of polymer-ion, ion-ion interactions. The deconvolution of the FTIR band associated with the anion reported that the free ion area is enhanced with the addition of salt which suggests the proper salt dissociation. The film PEO-PVP + $NaPF_6$ ($\ddot{O}/Na^+ = 8$) exhibits highest ionic conductivity $\sim 5.92 \times 10^{-6}$ S cm^{-1} at 40 °C and $\sim 2.46 \times 10^{-4}$ cm^{-1} at 100 °C. The temperature-dependent conductivity shows an Arrhenius type behavior and a decrease in activation energy evidence the increased flexibility and hence the enhanced ionic conductivity. DSC also supports the enhancement of the ionic conductivity as both T_g and T_m shifts toward lower temperature. The high temperature (100 °C) conductivity monitoring is done for the optimized PEO-PVP + $NaPF_6$ ($\ddot{O}/Na^+ = 8$) highly conductive system, and the conductivity can still be maintained stably up to 160 h (approx. 7 days). The prepared polymer electrolyte film displays the smoother surface in addition of salt and a thermal stability up to 300 °C. The high value of the ion transference number suggests that the present blend polymer electrolyte is totally ionic in nature. The improved conductivity, high ionic transference number, and broad voltage stability window support the use of prepared polymer electrolyte with long-term cycle stability and thermal stability for the solid-state sodium ion batteries.

References

1. Mizushima K, Jones PC, Wiseman PJ, Goodenough JB (1980) Li_xCoO_2 (0< x<−1): a new cathode material for batteries of high energy density. Mater Res Bull 15(6):783–789
2. Bella F, Muñoz-García AB, Meligrana G, Lamberti A, Destro M, Pavone M, Gerbaldi C (2017) Unveiling the controversial mechanism of reversible Na storage in TiO2 nanotube arrays: amorphous versus anatase TiO2. Nano Res 10(8):2891–2903
3. Placke T, Kloepsch R, Dühnen S, Winter M (2017) Lithium ion, lithium metal, and alternative rechargeable battery technologies: the odyssey for high energy density. J Solid State Electrochem 21(7): 1939–1964
4. Li Y, Lu Y, Zhao C, Hu YS, Titirici MM, Li H et al (2017) Recent advances of electrode materials for low-cost sodium-ion batteries towards practical application for grid energy storage. Energy Storage Mater 7:130–151
5. Peters J, Buchholz D, Passerini S, Weil M (2016) Life cycle assessment of sodium-ion batteries. Energy Environ Sci 9(5):1744–1751
6. Wessells CD, Peddada SV, Huggins RA, Cui Y (2011) Nickel hexacyanoferrate nanoparticle electrodes for aqueous sodium and potassium ion batteries. Nano Lett 11(12):5421–5425
7. Wang Y, Mu L, Liu J, Yang Z, Yu X, Gu L, Hu YS, Li H, Yang XQ, Chen L, Huang X (2015) A novel high capacity positive electrode material with tunnel-type structure for aqueous sodium-ion batteries. Adv Energy Mater 5(22):1501005
8. Pasta M, Wessells CD, Liu N, Nelson J, McDowell MT, Huggins RA, Toney MF, Cui Y (2014) Full open-framework batteries for stationary energy storage. Nat Commun 5:3007
9. Suo L, Borodin O, Wang Y, Rong X, Sun W, Fan X, Xu S, Schroeder MA, Cresce AV, Wang F, Yang C (2017) "Water-in-Salt" Electrolyte Makes Aqueous Sodium-Ion Battery Safe, Green, and Long-Lasting. Adv Energy Mater 7:1701189
10. Colo F, Bella F, Nair JR, Gerbaldi C (2017) Light-cured polymer electrolytes for safe, low-cost and sustainable sodium-ion batteries. J Power Sources 365:293–302
11. Singh V K, Singh S K, Gupta H, Balo L, Tripathi A K, Verma Y L, Singh R K (2018) Electrochemical investigations of Na0. 7CoO2 cathode with PEO-NaTFSI-BMIMTFSI electrolyte as promising material for Na-rechargeable battery. J Solid State Electrochem 1–11. DOI: 10.1007/s10008-018-3891-5
12. Srivastava N, Kumar M (2016) Ion dynamics and relaxation behavior of NaPF6-doped polymer electrolyte systems. J Solid State Electrochem 20(5):1421–1428
13. Fenton DE, Parker JM, Wright PV (1973) Complexes of alkali metal ions with poly(ethylene oxide). Polymer 14(11):589
14. Meyer WH (1998) Polymer electrolytes for lithium-ion batteries. Adv Mater 10(6):439–448
15. Sohn JY, Im JS, Shin J, Nho YC (2012) PVDF-HFP/PMMA-coated PE separator for lithium ion battery. J Solid State Electrochem 16(2):551–556
16. Prabakaran P, Manimuthu RP, Gurusamy S (2017) Influence of barium titanate nanofiller on PEO/PVdF-HFP blend-based polymer electrolyte membrane for Li-battery applications. J Solid State Electrochem 21(5):1273–1285
17. Bella F, Colò F, Nair JR, Gerbaldi C (2015) Photopolymer electrolytes for sustainable, upscalable, safe, and ambient-temperature sodium-ion secondary batteries. ChemSusChem 8(21):3668–3676
18. Sharma AL, Thakur AK (2011) AC conductivity and relaxation behavior in ion conducting polymer nanocomposite. Ionics 17(2): 135–143
19. Sharma AL, Thakur AK (2010) Polymer–ion–clay interaction based model for ion conduction in intercalation-type polymer nanocomposite. Ionics 16(4):339–350
20. Xu R, Huang X, Lin X, Cao J, Yang J, Lei C (2017) The functional aqueous slurry coated separator using polyvinylidene fluoride powder particles for lithium-ion batteries. J Electroanal Chem 786:77–85
21. Costa CM, Silva MM, Lanceros-Mendez S (2013) Battery separators based on vinylidene fluoride (VDF) polymers and copolymers for lithium ion battery applications. RSC Adv 3(29):11404–11417
22. Xie J, Zhang Q (2016) Recent progress in rechargeable lithium batteries with organic materials as promising electrodes. J Mater Chem A 4(19):7091–7106
23. Sadiq M, Arya A, Sharma AL (2016) Optimization of free standing polymer electrolytes films for lithium ion batteries application. Int Res Adv 3:16–20
24. Arya A, Sharma AL (2017) Insights into the use of polyethylene oxide in energy storage/conversion devices: a critical review. J Phys D Appl Phys 50(44):443002

25. Chowdhury FI, Khandaker MU, Amin YM, Arof AK (2017) Effect of gamma radiation on the transport and structural properties of polyacrylonitrile-lithium bis (oxalato) borate films. Solid State Ionics 304:27–39

26. Zhang C, Gamble S, Ainsworth D, Slawin AM, Andreev YG, Bruce PG (2009) Alkali metal crystalline polymer electrolytes. Nat Mater 8(7):580–584

27. Arya A, Sharma AL (2017) Polymer electrolytes for lithium ion batteries: a critical study. Ionics 23(3):497–540

28. Choi BK, Kim YW, Shin HK (2000) Ionic conduction in PEO–PAN blend polymer electrolytes. Electrochim Acta 45(8-9):1371–1374

29. Jacob MM, Prabaharan SR, Radhakrishna S (1997) Effect of PEO addition on the electrolytic and thermal properties of PVDF-LiClO$_4$ polymer electrolytes. Solid State Ionics 104(3-4):267–276

30. Arya A, Sharma S, Sharma AL, Dinesh K, Sadiq M (2016) Structural and dielectric behavior of blend polymer electrolyte based on PEO-PAN + LiPF$_6$. Asian J Eng App Tech 5(1):4–7

31. Fan L, Dang Z, Nan CW, Li M (2002) Thermal, electrical and mechanical properties of plasticized polymer electrolytes based on PEO/P (VDF-HFP) blends. Electrochim Acta 48(2):205–209

32. Joge P, Kanchan DK, Sharma P, Gondaliya N (2013) Effect of nano-filler on electrical properties of PVA-PEO blend polymer electrolyte. Indian J Pure Appl Phys 51:350

33. Ali TM, Padmanathan N, Selladurai S (2015) Effect of nanofiller CeO$_2$ on structural, conductivity, and dielectric behaviors of plasticized blend nanocomposite polymer electrolyte. Ionics 21:829–840

34. Premalatha M, Vijaya N, Selvasekarapandian S, Selvalakshmi S (2016) Characterization of blend polymer PVA-PVP complexed with ammonium thiocyanate. Ionics 22(8):1299–1310

35. Prasanna CS, Suthanthiraraj SA (2016) Electrical, structural, and morphological studies of honeycomb-like microporous zinc-ion conducting poly (vinyl chloride)/poly (ethyl methacrylate) blend-based polymer electrolytes. Ionics 22(3):389–404

36. Aravindan V, Vickraman P, Kumar TP (2007) ZrO$_2$ nanofiller incorporated PVC/PVdF blend-based composite polymer electrolytes (CPE) complexed with LiBOB. J Membr Sci 305(1-2):146–151

37. Ramesh S, Ramesh K, Arof AK (2013) Fumed silica-doped poly (vinyl chloride)-poly (ethylene oxide)(PVC/PEO)-based polymer electrolyte for lithium ion battery. Int J Electrochem Sci 8:8348–8355

38. Reddeppa N, Sharma AK, Rao VN, Chen W (2014) AC conduction mechanism and battery discharge characteristics of (PVC/PEO) polyblend films complexed with potassium chloride. Measurement 47:33–41

39. Nadimicherla R, Kalla R, Muchakayala R, Guo X (2015) Effects of potassium iodide (KI) on crystallinity, thermal stability, and electrical properties of polymer blend electrolytes (PVC/PEO: KI). Solid State Ionics 278:260–267

40. Arya A, Sharma AL (2016) Conductivity and stability properties of solid polymer electrolyte based on PEO-PAN+LiPF$_6$ for energy storage. App Sci Lett 2:72–75

41. Kumar A, Deka M (2012) PEO/P (VdF-HFP) blend based Li+ ion-conducting composite polymer electrolytes dispersed with dedoped (insulating) polyaniline nanofibers. J Solid State Electrochem 16(1):35–44

42. Reddy CVS, Zhu QY, Mai LQ, Chen W (2007) Electrochemical studies on PVC/PVdF blend-based polymer electrolytes. J Solid State Electrochem 11(4):543–548

43. Zhang X, Takegoshi K, Hikichi K (1992) High-resolution solid-state 13C nuclear magnetic resonance study on poly (vinyl alcohol)/poly (vinylpyrrolidone) blends. Polymer 33(4):712–717

44. Feng H, Feng Z, Shen L (1993) A high resolution solid-state nmr and dsc study of miscibility and crystallization behaviour of poly (vinyl alcohol) poly (N-vinyl-2-pyrrolidone) blends. Polymer 34(12):2516–2519

45. Polu AR, Kumar R, Rhee HW (2015) Magnesium ion conducting solid polymer blend electrolyte based on biodegradable polymers and application in solid-state batteries. Ionics 21(1):125–132

46. Kumar KK, Ravi M, Pavani Y, Bhavani S, Sharma AK, Rao VN (2011) Investigations on the effect of complexation of NaF salt with polymer blend (PEO/PVP) electrolytes on ionic conductivity and optical energy band gaps. Phys B: Cond Matt 406(9):1706–1712

47. Vondrák J, Reiter J, Velická J, Sedlaříková M (2004) PMMA-based aprotic gel electrolytes. Solid State Ionics 170(1-2):79–82

48. Hashmi SA, Upadhyaya HM, Thakur AK, Verma AL (2000) Experimental investigations on poly (ethylene oxide) based sodium ion conducting composite polymer electrolytes dispersed with SnO$_2$. Ionics 6(3-4):248–259

49. Song S, Kotobuki M, Zheng F, Xu C, Savilov SV, Hu N, Lu L, Wang Y, Li WD (2017) A hybrid polymer/oxide/ionic-liquid solid electrolyte for Na-metal batteries. J Mat Chem A 5(14):6424–6431

50. Luo H, Liang X, Wang L, Zheng A, Liu C, Feng J (2014) Highly mobile segments in crystalline poly (ethylene oxide) 8: NaPF6 electrolytes studied by solid-state NMR spectroscopy. J Chem Phys 140(7):074901

51. Bhatt C, Swaroop R, Arya A, Sharma AL (2015) Effect of nano-filler on the properties of polymer nanocomposite films of PEO/PAN complexed with NaPF$_6$. J Mater Sci Eng B 5:418–434

52. Koduru HK, Iliev MT, Kondamareddy KK, Karashanova D, Vlakhov T, Zhao XZ, Scaramuzza N (2016) Investigations on poly (ethylene oxide)(PEO)-blend based solid polymer electrolytes for sodium ion batteries. J Phys: Conf Series 764:012006

53. Roy A, Dutta B, Bhattacharya S (2017) Ion dynamics in NaBF$_4$ salt-complexed PVC–PEO blend polymer electrolytes: correlation between average ion hopping length and network structure. Ionics 1–11

54. Kumar KK, Ravi M, Pavani Y, Bhavani S, Sharma AK, Rao VN (2014) Investigations on PEO/PVP/NaBr complexed polymer blend electrolytes for electrochemical cell applications. J Membr Sci 454:200–211

55. Jamesh MI, Prakash AS (2018) Advancement of technology towards developing Na-ion batteries. J Power Sources 378:268–300

56. Kesavan K, Mathew CM, Rajendran S, Ulaganathan M (2014) Preparation and characterization of novel solid polymer blend electrolytes based on poly (vinyl pyrrolidone) with various concentrations of lithium perchlorate. Mate Sci Eng B 184:26–33

57. Kesavan K, Mathew CM, Rajendran S (2014) Lithium ion conduction and ion-polymer interaction in poly (vinyl pyrrolidone) based electrolytes blended with different plasticizers. Chin Chem Lett 25(11):1428–1434

58. Ma Y, Li LB, Gao GX, Yang XY, You Y (2016) Effect of montmorillonite on the ionic conductivity and electrochemical properties of a composite solid polymer electrolyte based on polyvinylidenedifluoride/polyvinyl alcohol matrix for lithium ion batteries. Electrochim Acta 187:535–542

59. Kumar KN, Kang M, Sivaiah K, Ravi M, Ratnakaram YC (2016) Enhanced electrical properties of polyethylene oxide (PEO)+ poly-vinylpyrrolidone (PVP): Li$^+$. Ionics 22(6):815–825

60. Das A, Thakur AK, Kumar K (2013) Exploring low temperature Li$^+$ ion conducting plastic battery electrolyte. Ionics 19(12):1811–1823

61. Sharma AL, Shukla N, Thakur AK (2008) Studies on structure property relationship in a polymer–clay nanocomposite film based on (PAN)$_8$LiClO$_4$. J Polym Sci B Polym Phys 46(23):2577–2592

62. Sharma AL, Thakur AK (2013) Plastic separators with improved properties for portable power device applications. Ionics 19(5):795–809

63. Das S, Ghosh A (2017) Charge carrier relaxation in different plasticized PEO/PVDF-HFP blend solid polymer electrolytes. J Phys Chem B 121(21):5422–5432

64. Vijaya N, Selvasekarapandian S, Karthikeyan S, Prabu M, Rajeswari N, Sanjeeviraja C (2013) Synthesis and characterization of proton conducting polymer electrolyte based on poly (N-vinyl pyrrolidone). J Appl Polym Sci 127(3):1538–1543

65. Burba CM, Frech R (2005) Spectroscopic measurements of ionic association in solutions of $LiPF_6$. J Phys Chem B 109(31):15161–15164

66. Sharma AL, Thakur AK (2011) Polymer matrix–clay interaction mediated mechanism of electrical transport in exfoliated and intercalated polymer nanocomposites. J Mater Sci 46(6):1916–1931

67. Ni'mah YL, Cheng MY, Cheng JH, Rick J, Hwang BJ (2015) Solid-state polymer nanocomposite electrolyte of TiO_2/PEO/$NaClO_4$ for sodium ion batteries. J Power Sources 278:375–381

68. Tang R, Jiang C, Qian W, Jian J, Zhang X, Wang H, Yang H (2015) Dielectric relaxation, resonance and scaling behaviors in $Sr_3Co_2Fe_{24}O_{41}$ hexaferrite. Sci Rep 5:13645

69. Jonscher AK (1983) Dielectric relaxation in solids. Chelsea Dielectric, London

70. Anilkumar KM, Jinisha B, Manoj M, Jayalekshmi S (2017) Poly (ethylene oxide)(PEO)–Poly (vinyl pyrrolidone)(PVP) blend polymer based solid electrolyte membranes for developing solid state magnesium ion cells. Eur Polym J 89:249–262

71. Arya A, Sharma AL (2018) Structural, electrical properties and dielectric relaxations in Na+ ion conducting solid polymer electrolyte. J Phys Condens Matter 30:165402

72. Chilaka N, Ghosh S (2014) Dielectric studies of poly (ethylene glycol)-polyurethane/poly (methylmethacrylate)/montmorillonite composite. Electrochim Acta 134:232–241

73. Reddy Polu A, Kumar R (2011) Impedance spectroscopy and FTIR studies of PEG-based polymer electrolytes. J Chem 8:347–353

74. Naveen Kumar P, Sasikala U, Sharma AK (2013) Investigations on conductivity and discharge profiles of novel (PEO+PEMA) polymer blend electrolyte. Int J Inno Res Sci Eng Tech 2:3575–3582

75. Koduru HK, Marino L, Scarpelli F, Petrov AG, Marinov YG, Hadjichristov GB, Iliev MT, Scaramuzza N (2017) Structural and dielectric properties of $NaIO_4$–Complexed PEO/PVP blended solid polymer electrolytes. Curr App Phys 17:1518–1531

76. Ramamohan K, Umadevi C, Achari VB, Sharma AK (2013) Conductivity studies on (PVC/PEMA) solid polymer blend electrolyte films complexed with $NaIO_4$. Int J Plas Tech 17:139–148

77. Deraman SK, Mohamed NS, Subban RH (2013) Conductivity and electrochemical studies on polymer electrolytes based on poly vinyl (chloride)-ammonium triflate-ionic liquid for proton battery. Int J Electrochem Sci 8:1459–1468

78. Laha P, Panda AB, Dahiwale S, Date K, Patil KR, Barhai PK, Das AK, Banerjee I, Mahapatra SK (2010) Effect of leakage current and dielectric constant on single and double layer oxides in MOS structure. Thin Solid Films 519(5):1530–1535

79. Latif F, Aziz M, Katun N, Yahya MZ (2006) The role and impact of rubber in poly (methyl methacrylate)/lithium triflate electrolyte. J Power Sources 159:1401–1404

80. Mohamad AA, Mohamed NS, Yahya MZ, Othman R, Ramesh S, Alias Y, Arof AK (2003) Ionic conductivity studies of poly (vinyl alcohol) alkaline solid polymer electrolyte and its use in nickel–zinc cells. Solid State Ionics 156:171–177

81. Arof AK, Amirudin S, Yusof SZ, Noor IM (2014) A method based on impedance spectroscopy to determine transport properties of polymer electrolytes. Phys Chem Chem Phys 16:1856–1867

82. Arya A, Sadiq M, Sharma AL (2017) Effect of variation of different Nano filler on structural, electrical, dielectric and transport properties of blend polymer nanocomposites. Ionics. https://doi.org/10.1007/s11581-017-2364-7

83. Arya A, Sharma AL (2017) Structural microstructural and electrochemical properties of dispersed type polymer nanocomposite films. J Phys D Appl Phys 51:045504

84. Kim S, Park SJ (2007) Preparation and ion-conducting behaviors of poly (ethylene oxide)-composite electrolytes containing lithium montmorillonite. Solid State Ionics 178:973–979

85. Laha P, Panda AB, Mahapatra SK, Barhai PK, Das AK, Banerjee I (2012) Development of rf plasma sputtered Al_2O_3–TiO_2 multilayer broad band antireflecting coatings and its correlation with plasma parameters. Appl Surf Sci 258:2275–2282

86. Dey A, Karan S, De SK (2013) Effect of nanoadditives on ionic conductivity of solid polymer electrolyte. Indian J Pure Appl Phys 51:281–288

87. Jinisha B, Anilkumar KM, Manoj M, Pradeep VS, Jayalekshmi S (2017) Development of a novel type of solid polymer electrolyte for solid state lithium battery applications based on lithium enriched poly (ethylene oxide)(PEO)/poly (vinyl pyrrolidone)(PVP) blend polymer. Electrochim Acta 235:210–222

88. Ramesh S, Teh GB, Louh RF, Hou YK, Sin PY, Yi LJ (2010) Preparation and characterization of plasticized high molecular weight PVC-based polymer electrolytes. Sadhana 35:87–95

89. Yang CC (2002) Polymer Ni–MH battery based on PEO–PVA–KOH polymer electrolyte. J Power Sources 109:22–31

90. Zhang Y, Zhao Y, Gosselink D, Chen P (2015) Synthesis of poly (ethylene-oxide)/nanoclay solid polymer electrolyte for all solid-state lithium/sulfur battery. Ionics 21:381–385

91. Sharma AL, Thakur AK (2010) Improvement in voltage, thermal, mechanical stability and ion transport properties in polymer-clay nanocomposites. J Appl Polym Sci 118:2743–2753

92. Yadav N, Mishra K, Hashmi SA (2017) Optimization of porous polymer electrolyte for quasi-solid-state electrical double layer supercapacitor. Electrochim Acta 235:570–582